Université de Neuchâtel
Institut de Microtechnique

Diffractive optical elements for interconnections

Thèse

sous forme réduite

Présentée à la Faculté des sciences
pour obtenir le grade de docteur ès sciences

par

Damien Prongué

Neuchâtel, août 1992

IMPRIMATUR POUR LA THÈSE

Diffractive optical elements for interconnections

de M.onsieur Damien Prongué

UNIVERSITÉ DE NEUCHÂTEL

FACULTÉ DES SCIENCES

La Faculté des sciences de l'Université de Neuchâtel
sur le rapport des membres du jury,

Messieurs R. Dändliker, H. Hügli, H. Buczek (Marin), M.T. Gale (Inst. P. Scherrer, Zurich) et J. Jahns (AT&T Bell Lab., Holmdel, USA)

autorise l'impression de la présente thèse.

Neuchâtel, le 9 juillet 1992

Le doyen:

A. Robert

JAPANESE JOURNAL OF APPLIED PHYSICS
VOL. 29, NO. 7, JULY, 1990, pp. L 1307–L 1309

Design and Fabrication of Highly Efficient Fan-Out Elements

H. P. HERZIG, D. PRONGUÉ and R. DÄNDLIKER

Institute of Microtechnology, University of Neuchâtel, Rue A.-L. Breguet 2, CH-2000 Neuchâtel, Switzerland

(Received March 26, 1990; accepted for publication May 19, 1990)

This paper reports the calculation and fabrication of periodic phase structures for fan-out elements with a theoretical conversion efficiency close to 100% and perfect uniformity. We have measured an efficiency of 92% for a smooth kinoform structure fabricated in photoresist by laser beam writing lithography.

KEYWORDS: fan-out, kinoform, phase grating, Dammann grating, CGH, HOE

Optical fan-out elements split a single laser beam into a one- or two-dimensional array of beams. Fan-out elements are key components in many applications of modern optics, such as parallel optical processing and fiber optic communication. Similar elements can also be used for beam shaping of laser diode arrays.[1] Binary phase gratings, also called Dammann gratings,[2] represent a successful technique to fabricate fan-out elements with good uniformity of the generated array of beams, but moderate efficiency (60%–70%). More recently, efforts are concentrated on kinoforms in order to increase the diffraction efficiency. This paper deals with the calculation and fabrication of smooth periodic phase structures as fan-out elements with a theoretical conversion efficiency (single-beam/multi-beam) close to 100%. In addition, the presented design method requires only low computing power, even for very large fan-outs.

A fan-out element can be considered as far-field hologram of a one- or two-dimensional array of coherent light sources (Fig. 1). The light sources of the array, spaced by the distance s, are characterized by their amplitudes and phases, A_i and ϕ_i. For a linear array of N point sources on the x-axis we can write the near-field amplitude distribution $U(x, y)$ as

$$U(x, y)=\sum_{m=1}^{N} A_m \exp [i\phi_m]\delta(x-x_m, y), \tag{1}$$

with $x_{m+1}-x_m=s$.

The far-field distribution $\hat{U}(u, v)$ is related to the near field $U(x, y)$ by a Fourier transformation. Thus, we get for the far-field

$$\begin{aligned}\hat{U}(u, v)&=\sum_{m=1}^{N} A_m \exp [i\phi_m] \exp [2\pi i x_m u]\\ &=|\hat{U}(u, v)| \exp [i\Psi(u, v)],\end{aligned} \tag{2}$$

where $\Psi(u, v)=\arg\{\hat{U}\}$. In the far-field intensity distribution we can observe interference patterns with periodicities of $1/s$, $1/2s\cdots$, described by[1]

$$I(u, v)=|\hat{U}|^2=\sum_{m=1}^{N} A_m^2+2\sum_{k=1}^{N-1} B_k \cos [2\pi ksu+\Phi_k]. \tag{3}$$

For a given set A_i, ϕ_i, the intermodulation terms B_k can be calculated by

$$\sum_k B_k \cos [2\pi ksu+\Phi_k]$$

$$=\sum_{n<m} A_m A_n \cos [2\pi u(m-n)s+(\phi_m-\phi_n)], \tag{4}$$

where $k=m-n$ and $n<m=1\cdots N$.

The corresponding hologram, considered as a phase grating with $\Psi(u, v)$ of eq. (2), becomes only efficient, if these intermodulation terms are minimized, otherwise part of the input energy is diffracted into undesired beams. Minimum power of the intermodulation in eq. (3) means that

$$\int_{-\infty}^{\infty}\int_{-\infty}^{\infty}\left(\sum_k B_k \cos [2\pi ksu+\Phi_k]\right)^2 du\, dv\rightarrow\min. \tag{5}$$

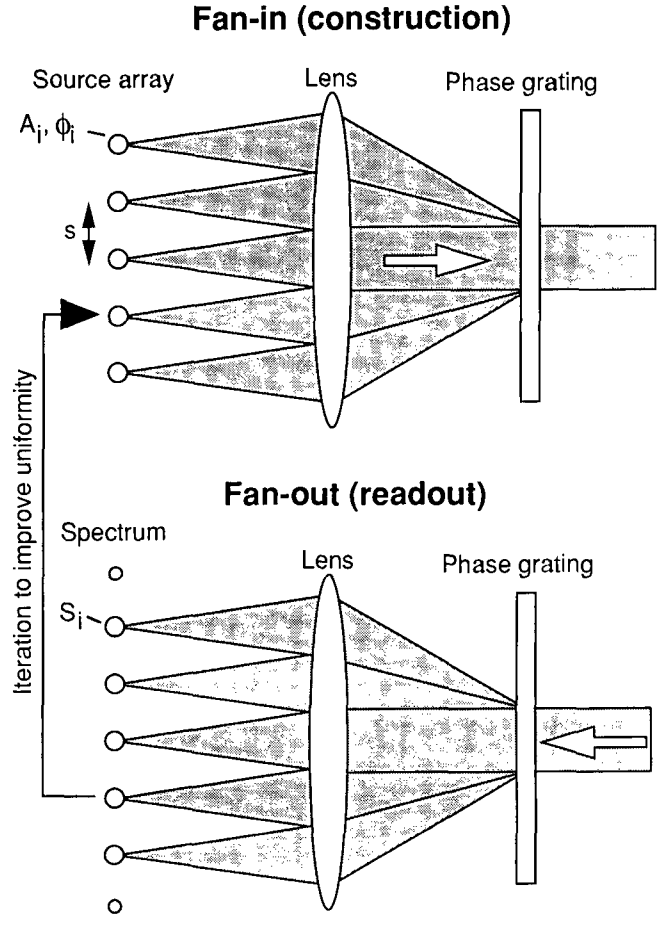

Fig. 1. Construction and read-out of fan-out elements.

As the terms with different spatial frequencies are orthogonal, the minimum condition becomes finally

$$\sum_k B_k^2 \rightarrow \min. \tag{6}$$

This can be achieved by appropriate choice of the phases φ_i, obtained by numerical optimization.[1)]

This consideration is independent of the technology used to fabricate the phase element, it holds as well for surface relief elements (kinoforms) as for volume holograms. The fan-out corresponds to the spectrum of the phase grating (Fig. 1). In general, the amplitudes S_i in the (calculated) spectrum will be different from the initial A_i. However, by iteration the uniformity can be improved.

Figure 2 shows the spectrum of an optimized smooth phase grating for a linear fan-out element which generates $N=9$ beams of equal intensity. The conversion efficiency is 99.3% and the uniformity is perfect. To calculate the optimum fan-out element, we start with the amplitudes $A_i=1$ and optimize the efficiency by varying the phases ϕ_i. Then, the spectrum of the corresponding phase grating is calculated, yielding the amplitudes S_i generated in the readout (Fig. 1). In general, they are different from the desired values for a uniform fan-out, which is $S_i=1$ for $i=1\cdots N$. By iteration, i.e. by increasing or decreasing the amplitude A_i if the corresponding S_i is smaller or larger than 1, a perfect solution is found after a few steps. Efficiencies close to 100% can be achieved for nearly any fan-out with $N>6$.

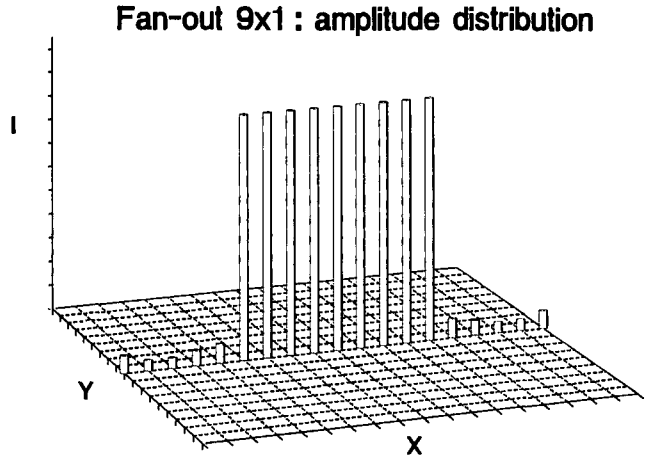

Fig. 2. Spectrum of an optimized smooth phase grating for a linear fan-out element, which generates 9 beams of equal intensity. The conversion efficiency is 99.3% and the uniformity is perfect.

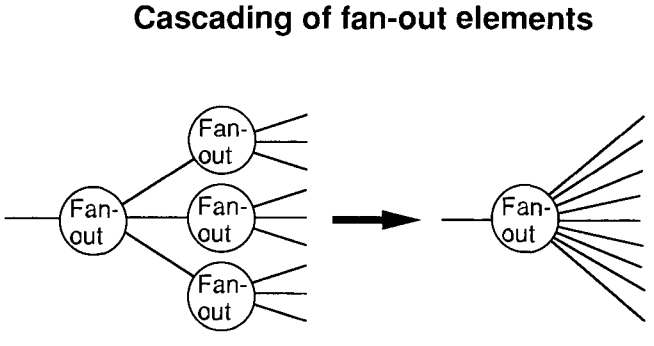

Fig. 3. Cascading of fan-out elements.

Large fan-out elements with high efficiency can be constructed with negligible computing time by cascading the solutions found for smaller fan-out elements as shown in Fig. 3. For example, we can start with an optimized fan-out element generating a linear array ($N=9$) characterized by the parameters A_i and ϕ_i (Fig. 1). By cascading, we get a much larger array with $N=9^2=81$, characterized now by $A_k=A_iA_j$ and $\phi_k=\phi_i+\phi_j$ with $i, j=1\cdots N$. This method can be generalized by multiple cascading and by combining arrays of different sizes. In general, the resulting elements will still have a very high efficiency (close to 100%), however, the uniformity of the fan-out becomes bad, so that additional iteration is necessary to restore it.

Figure 4 shows the spectrum of an optimized phase structure for a 2-dimensional fan-out element, which generates 9×9 beams of equal intensity. The conversion efficiency is 99.3% and the uniformity is perfect. This element has been calculated by crossing two linear fan-out elements. Crossing means cascading two linear arrays which are perpendicular to each other, in order to generate a 2-dimensional array. As is described above, the characteristic parameters are then given by $A_k=A_iA_j$ and $\phi_k=\phi_i+\phi_j$ with $i, j=1\cdots N$. Crossing has the advantage that the uniformity of the fan-out is conserved, because the two dimensions are independent.

After all, for this type of fan-out elements the fabrication becomes the limiting factor for the efficiency and the uniformity. A very promising approach is to fabricate the phase structure by laser beam writing lithography as smooth relief grating in photoresist. We used the design of a fan-out element, which is highly efficient (99.3%) but not completely uniform (±5% theoretically), to fabricate a corresponding kinoform in collaboration with the PSI/RCA Laboratories.[3)] The profile of the developed photoresist relief shown in Fig. 5 has been measured mechanically. The grating period is $\Lambda=500\ \mu$m

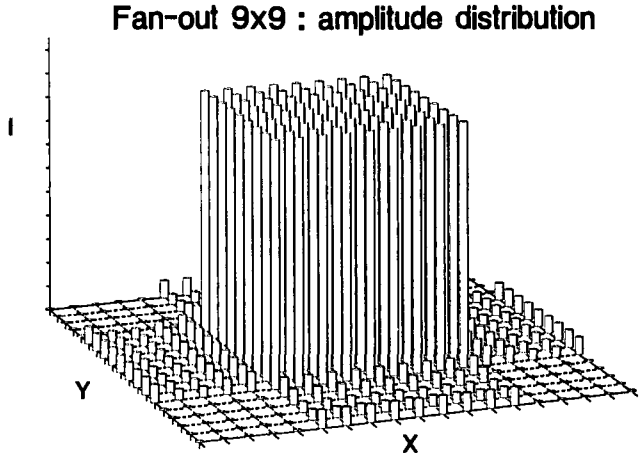

Fig. 4. Spectrum of an optimized phase grating for a 2-dimensional fan-out element, which generates 9×9 beams of equal intensity. The conversion efficiency is 99.3% and the uniformity is perfect.

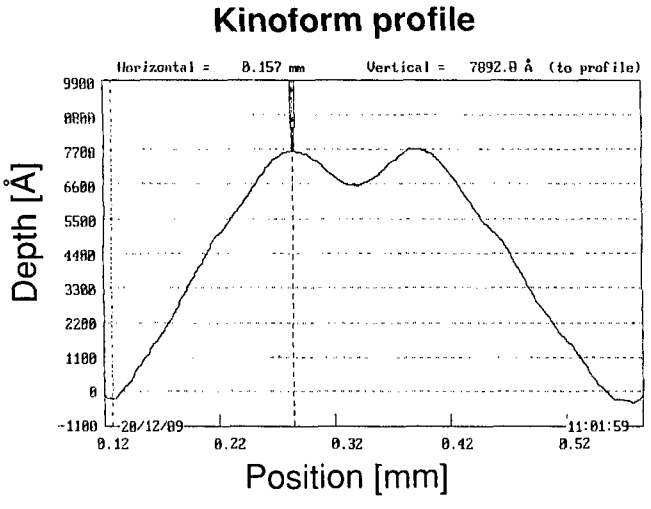

Fig. 5. Profile of the smooth relief grating in photoresist, fabricated in collaboration with the PSI/RCA Laboratories by laser beam writing lithography.[3]

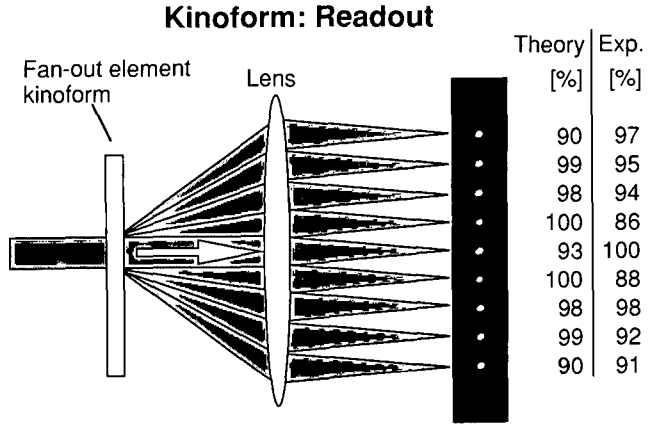

Fig. 6. Spectrum of the smooth fan-out element (Fig. 5) at $\lambda = 488$ nm. The experimental results yield an efficiency of 92% (99.3% theoretical) and intensity variations of ±7% (±5% theoretical).

and the measured depth of 0.77 μm corresponds well to the desired value. The photoresist relief structure can be converted into a metal master relief by electroplating techniques for mass-production of low-cost replicas.

To test the fan-out, we have illuminated the phase grating described above (Fig. 5) with a plane wave from an argon laser ($\lambda = 488$ nm). The smooth kinoform element generates 9 fan-out beams (Fig. 6) containing 92% of the total light power transmitted through the element. We have measured intensity variations of ±7%. The corresponding spots have been detected with a CCD camera. For comparison, the theoretical and the experimental values for the relative intensities of the fan-out beams are given. The theoretical results for the design described in Fig. 5 are 99.3% for the efficiency and ±5% for the uniformity.

Another method to fabricate fan-out elements uses a computer-generated hologram (CGH) to produce an array of coherent sources with optimized phases for minimum intermodulation, which can be used to record efficient holographic optical elements (HOE) as volume phase gratings in dichromated gelatine or photopolymer. This holographic recording technique allows also to include focussing power into the fan-out element. A similar phase structure as shown in Fig. 5, with a period of $\Lambda = 96\,\mu$m, has been encoded as CGH and then fabricated by electron beam lithography at the CSEM.[4] The carrier frequency of the CGH is $\nu = 250$ lines/mm, sufficient to separate the different diffraction orders. Illuminated with a laser beam at $\lambda = 488$ nm, the first

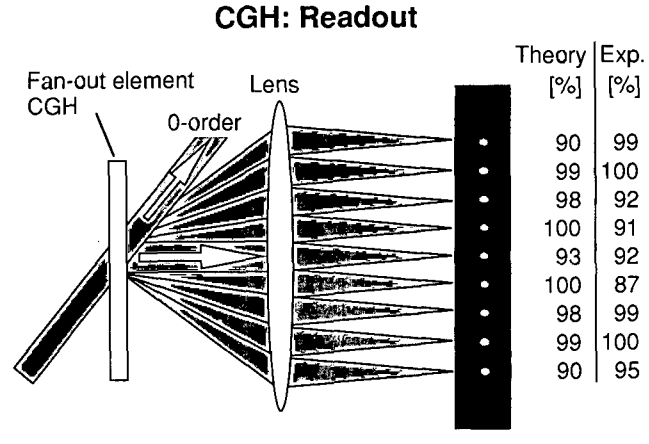

Fig. 7. Spectrum of the CGH fan-out at $\lambda = 488$ nm. The measured uniformity is within ±7%. The CGH has been fabricated by electron beam lithography at the CSEM.[4]

diffraction order of the CGH generates the desired array of sources (Fig. 7). The measured uniformity is within ±7%.

References

1) H. P. Herzig, R. Dändliker and J. M. Teijido: Holographic Systems, Components and Applications, Bath, UK, Conference Publication No. 311 (IEE, 1989) 133.
2) H. Dammann and K. Görtler: Opt. Commun. **3** (1971) 312.
3) M. T. Gale and K. Knop: Proc. Soc. Photo-Opt. Instrum. Eng. **398** (1983) 347.
4) H. Buczek and J. M. Teijido: Proc. Soc. Photo-Opt. Instrum. Eng. **884** (1988) 46.

PROCEEDINGS PREPRINT

SPIE–The International Society for Optical Engineering

Preprinted from

Holographic Optics III: Principles and Applications

11-15 March 1991
The Hague, The Netherlands

Volume 1507

Fan-out elements by multiple beam recording in volume holograms

H. P. Herzig, P. Ehbets, D. Prongué, R. Dändliker

Institute of Microtechnology, University of Neuchâtel, Rue A.-L. Breguet 2, CH-2000 Neuchâtel, Switzerland

ABSTRACT

The recording of efficient fan-out elements as volume holograms has been studied by using coupled wave theory. We have found that the efficiency and uniformity of regular fan-out elements depend strongly on the relative phases of the object waves, if the thickness t of the holographic emulsion is smaller than $t < \lambda/(n \tan\theta_0 \Delta\alpha)$. High efficiency and uniformity can be achieved by optimized phases of the object beams, thereby requiring a low dynamic range of the holographic recording material.

1. INTRODUCTION

Optical fan-out elements split a single laser beam into a regular array of equally intense light spots in one- or two-dimensions. They are used in many applications of modern optics, such as parallel optical processing and fiber optic communication. This paper deals with the recording of efficient fan-out elements in thick volume holograms. We have applied coupled wave theory to study the conditions for high diffraction efficiency and uniformity of the generated array of beams.

Papers about coupled wave theory for multiple beam recording predict high efficiency for replaying N waves, and only weak dependence of interactions between the beams due to the highly selective Bragg condition.[1] This would suggest that the recording of fan-out elements is an easy task. However, experimental results show the difficulties for recording uniform fan-out elements as volume holograms and the precaution necessary to generate a uniform distribution of the irradiance in the hologram plane.[2] The fundamental problems are explained in terms of recording non-linearity. Using coupled wave theory, we have found that also for perfect linearity the hologram does not generate a uniform fan-out. We will demonstrate how to apply coupled wave theory to the special problem of regular fan-out elements. These elements are called degenerated, because all gratings with equal periodicity diffract light in the same direction and must be added coherently. As a consequence, the results for efficiency and uniformity depend strongly on the relative phases of the recorded object waves.

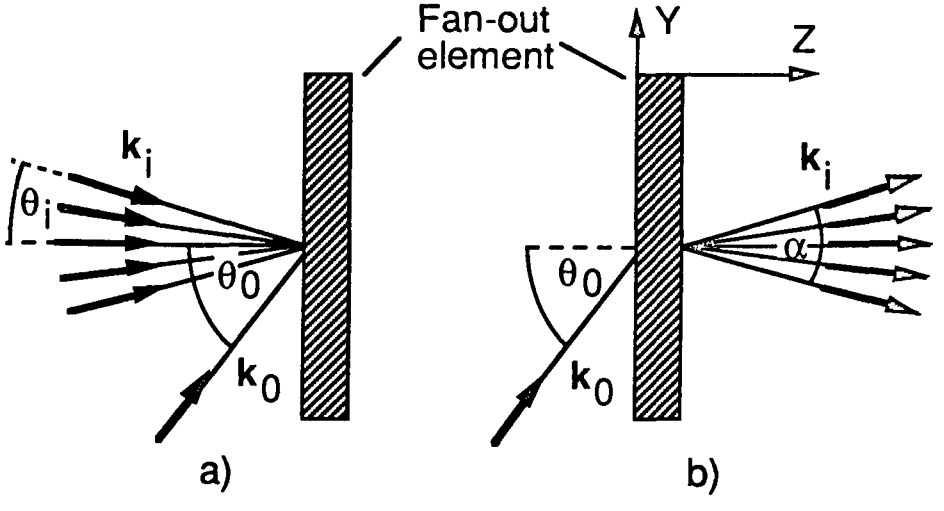

Fig. 1.
a) Recording and b) readout of fan-out elements. The angles are defined inside the recording medium with refractive index $n = \sqrt{\varepsilon_a}$ *(see Eq. 1).*

2. SIMULTANEOUS RECORDING WITH MINIMUM INTERMODULATIONS

A fan-out elements can be fabricated by recording a hologram of N object waves $E_i(\mathbf{x}) = A_i \exp\{-j\mathbf{k}_i \mathbf{x} + j\phi_i\}$ with a reference wave $E_0(\mathbf{x}) = A_0 \exp\{-j\mathbf{k}_0 \mathbf{x} + j\phi_0\}$. The waves are characterized by the wavevectors $\mathbf{k}_i = (k_i^y, k_i^z)$, amplitudes A_i and phases ϕ_i, $\mathbf{x} = (y,z)$ are the coordinates (Fig. 1). Only the s polarization is considered.

We assume, that the recording material responds linearly to the accumulated energy during exposure, i.e.

$$\varepsilon(y,z) = \varepsilon_a + \delta \left| \sum_{i=1}^{N} E_i + E_0 \right|^2 . \tag{1}$$

The dielectric permittivity $\varepsilon(y,z)$ after exposure becomes then

$$\varepsilon(y,z) = \varepsilon_a + \sum_{i=1}^{N} \Delta\varepsilon_{0i} \cos(\mathbf{K}_{0i} \mathbf{x} - \Phi_{0i}) + \sum_{q>p=1}^{N} \Delta\varepsilon_{pq} \cos(\mathbf{K}_{pq} \mathbf{x} - \Phi_{pq}) , \tag{2}$$

where $\Phi_{pq} = \phi_p - \phi_q$ and $\Delta\varepsilon_{pq} = 2\delta A_p A_q$. Besides the desired N primary gratings $\mathbf{K}_{0i} = \mathbf{k}_0 - \mathbf{k}_i$, $N(N-1)/2$ unwanted intermodulation gratings $\mathbf{K}_{pq} = \mathbf{k}_p - \mathbf{k}_q$ are recorded. At readout, they generate intermodulation waves, which are coupled with the desired reconstructed beams. As a consequence, efficiency and uniformity of the fanout suffer.

One possibility to reduce the intermodulations with respect to the primary gratings is to increase the reference-to-object beam ratio B, defined by[1]

$$B = \frac{A_0^2}{\sum_{i=1}^{N} A_i^2} . \tag{3}$$

Then, the modulations of the desired primary gratings become dominant ($\Delta\varepsilon_{0i} >> \Delta\varepsilon_{pq}$). Unfortunately this method requires a very high dynamic range of the recording material.

It has been shown earlier, that for on-axis regular fan-out elements the intermodulation gratings can be eliminated nearly perfectly.[3] In the case of regular elements, the projections K_{pq}^y of the grating vector $\mathbf{K}_{pq}$ in the hologram plane (y-axis) are all integer multiples of the lowest frequency $2\pi v$ formed by the interference between two neighboring object beams. Thus, we can write the intermodulation term in Eq. (2) as

$$\sum_{q>p}^{N} \Delta\varepsilon_{pq} \cos(\mathbf{K}_{pq} \mathbf{x} - \Phi_{pq}) = \sum_{q>p}^{N} \Delta\varepsilon_{pq} \cos(2\pi m v y + K_{pq}^z z - \Phi_{pq}), \tag{4}$$

where $m = p - q$. There are $N - 1$ gratings with $m = 1$, $N - 2$ gratings with $m = 2$, etc. By adding the gratings with the same frequency, but optimized phase shifts Φ_{pq}, one can minimize the intermodulations.[3]

Note, that the intermodulations vary in the z-direction with K_{pq}^z [Eq. (4)]. As a consequence, they can be minimized only for one specific plane parallel to the hologram plane (z = const). For on-axis fan-out

elements, shown in Fig. 1, the z-variation is rather slow, i.e. K_{pq}^{z} is small. The largest component K_{pq}^{z} is formed by the interference between the central beam, propagating in the direction of the z-axis, and the marginal beams of the fan-out. We obtain

$$(K_{pq}^{z})_{max} = \frac{2\pi}{\lambda} n(1 - \cos\frac{\alpha}{2}) = \frac{2\pi}{\Lambda}, \tag{5}$$

where λ is the wavelength, α the full angle $(\mathbf{k}_1,\mathbf{k}_N)$ of the fan-out, n the refractive index, and Λ the periodicity of the grating $(K_{pq}^{z})_{max}$. The intermodulations remain small within a depth h of $\pm \Lambda/10$, i.e.

$$h = \frac{\Lambda}{5} = \frac{\lambda}{5n(1 - \cos(\alpha/2))} . \tag{6}$$

We can conclude, that the hologram plane must be normal to the z-axis, within the tolerances given by Eq. (6). This restricts the permitted recording geometry.

For very thick holograms the off-Bragg interactions become negligible and therefore the phases of the object waves are irrelevant. In this case the recording geometry is not restricted by Eq. (6).

3. COUPLED WAVE EQUATIONS

In the following, we will derive the coupled wave equations for regular fan-out elements. The electrical field has to fulfill the Helmholtz equation

$$\Delta E(y,z) + k^2 \varepsilon(y,z) E(y,z) = 0, \tag{7}$$

with $k = (2\pi/\lambda)$ and $\varepsilon(y,z)$ is determined by Eq. (2).

The total electric field inside the hologram is written as a sum of M plane waves diffracted in different directions

$$E(y,z) = E_0(y,z) + \sum_{i=1}^{N} E_i(y,z) + \sum_{i=N+1}^{M} E_i(y,z) , \tag{8}$$

where the first N waves are the object waves. Each component of the electric field is of the form

$$E_i(y,z) = B_i(z) \exp\{-j\mathbf{k}_i \mathbf{x}\}, \tag{9}$$

where $B_i(z)$ are complex amplitudes.

The waves $E_i(y,z)$ are generated by diffraction of an incident beam $(\mathbf{k}_m)$ at a grating $\mathbf{K}_{pq}$. The wavevectors $\mathbf{k}_i$ are then determined by the beta-value construction, namely

$$k_i^{y} = k_m^{y} - K_{pq}^{y}, \qquad q > p = 0,\ldots,N-1;\ \ i,m = 1,\ldots,M. \tag{10}$$

For the z-components we obtain

$$k_i^{z} = \sqrt{k^2 \varepsilon_a - (k_i^{y})^2} . \tag{11}$$

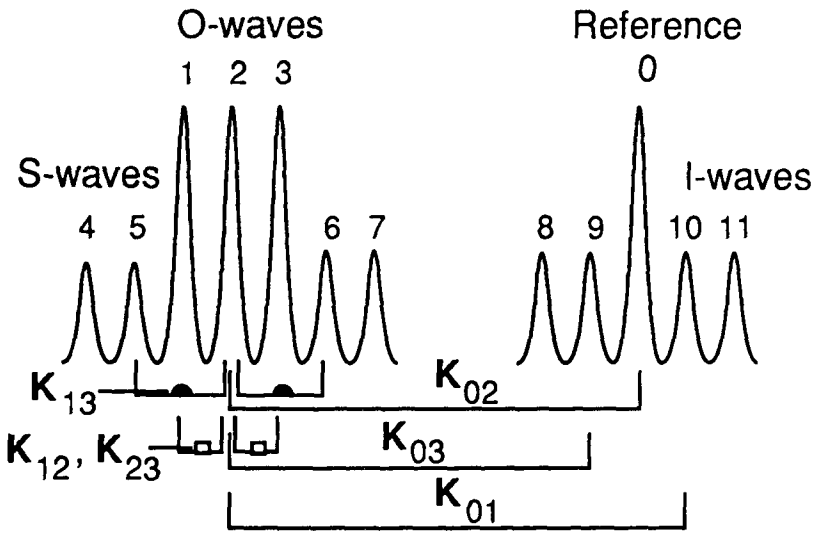

Fig. 2. Spectrum of the waves included in our model for a fan-out of N = 3 and possible interactions for O-wave no. 2 through primary gratings K_{0i} and intermodulation gratings K_{pq}.

The coupled wave equations are now obtained by introducing the electric field [Eq. (8)], into the Helmholtz equation (7) . This yields

$$\frac{dC_m}{dz}\cos\theta_m = \sum_n M_{mn}\, C_n, \tag{12}$$

where $C_i = B_i \exp\{-jk_i^z\}$. The reason for this substitution is to separate the wave parameters, described by the coefficients C_i, and the independent grating parameters, described by the matrix M_{mn}. Note, that the matrix must be hermitian, i.e. $M_{mn} = M_{nm}^*$.

For a simple coupling between two waves E_m and E_n through one grating K_{pq}, we get

$$M_{mn} = \chi_{pq} = \kappa_{pq} \exp\{j(-K_{pq}^z + \Phi_{pq})\}. \tag{13}$$

$\kappa_{pq} = k\Delta\varepsilon_{pq}/4$ is Kogelnik's coupling coefficient for the grating K_{pq}. Note, that the sign of $-K_{pq}^z$ stands for the first diffraction order.

We have to consider that each beam E_m diffracts at all gratings. In our degenerated case all gratings with equal periodicity, i.e. equal K_{pq}^y, diffract light in the same direction. Their coupling coefficients have to be added coherently, as shown in Eq. (14), which yields

$$M_{mn} = \sum \chi_{pq}\,, \qquad \text{for } q - p = \text{const.} \tag{14}$$

Figure 2 shows the spectrum of the electric field given by Eq. (8). We have made the following assumptions for our coupled wave model:

- Simultaneous recording of N object waves and one reference wave leads to N primary gratings $\mathbf{K}_{0i}$ and N(N – 1)/2 intermodulation gratings $\mathbf{K}_{pq}$, q > p = 1,...,(N – 1).
- The primary gratings are thick, only one diffraction order is considered.
- The intermodulation gratings are considered to be optically thin, the ± first diffraction orders are included.
- At readout, N object waves (O-waves), 2(N – 1) secondary waves (S-waves) and 2(N – 1) intermodulation waves (I-waves) are generated.
- Any possible coupling between the waves E_m through the gratings $\mathbf{K}_{0i}$ and $\mathbf{K}_{pq}$ are accepted.
- Coupling coefficients χ_{pq} of gratings with equal periodicity, i.e. equal $K_{pq}{}^{y}$, are added coherently.

4. NUMERICAL RESULTS

The coupled wave equations (12) have been solved by numerical integration using Runge-Kutta. The boundary conditions for transmission holograms at z = 0 are: $C_0 = 1$ and $C_i = 0$ for i = 1,...,M.

The diffraction efficiency η_T of all object waves is obtained from Eq. (15):

$$\eta_T = \sum_{i=1}^{N} \eta_i , \qquad \text{with} \qquad \eta_i = \frac{\cos\theta_i}{\cos\theta_0} \left| C_i \right|^2, \quad i = 1,...,N. \tag{15}$$

The signal to noise ratio SNR is defined as

$$\text{SNR} = \frac{\eta_T}{\eta_P}, \qquad \text{with} \qquad \eta_P = \sum_{i=N+1}^{M} \eta_i . \tag{16}$$

η_p is the total diffraction efficiency of all the parasitic waves. Important for fan-out elements is the uniformity error e described by

$$e = \frac{\eta_{i\max} - \eta_{j\min}}{< \eta_i >} . \tag{17}$$

In the following, we distinguish between the corrected and the uncorrected case. The corrected case has optimized phases Φ_{pq} for minimum intermodulations. Except in the trivial case of 3 waves, the phases Φ_{pq} have been determined by numerical optimization.[3] In the uncorrected, worst case, a constant phase is assumed. The following values have been used for the calculations:

- For 3 object beams: $\phi_1 = \phi_3 = 0$, $\phi_2 = \pi/2$.
- For 9 object beams: $\phi_1 = \phi_9 = 1.7722$, $\phi_2 = \phi_8 = 0.1351$, $\phi_3 = \phi_7 = 3.8871$, $\phi_4 = \phi_6 = 2.4547$, $\phi_5 = 3.1416$ ([rad]).
- Uncorrected, worst case: $\phi_i = 0$.

Note, that $\Phi_{pq} = \phi_p - \phi_q$.

Figure 3 shows the total useful diffraction efficiency for the corrected and the worst case as a function of the modulation amplitude of a single primary grating. In the following tables 1-4, the output parameters at the point of maximum diffraction efficiency η_T are compared. The angular separation of the on-axis fanout element is indicated by the angle $\Delta\alpha = \theta_{i+1} - \theta_i$ between two neighboring object beams.

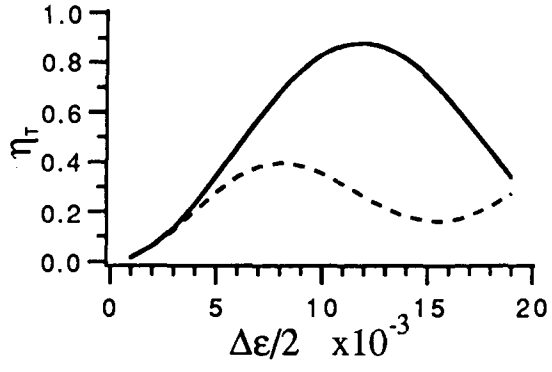

(a)

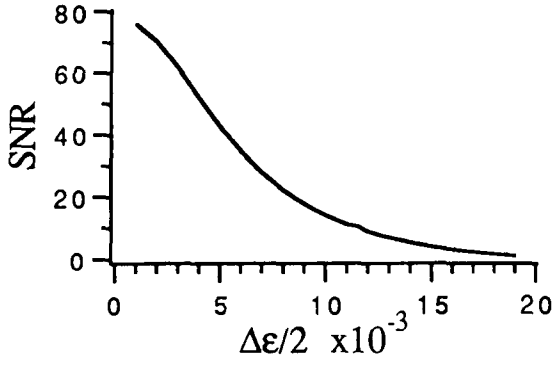

(b)

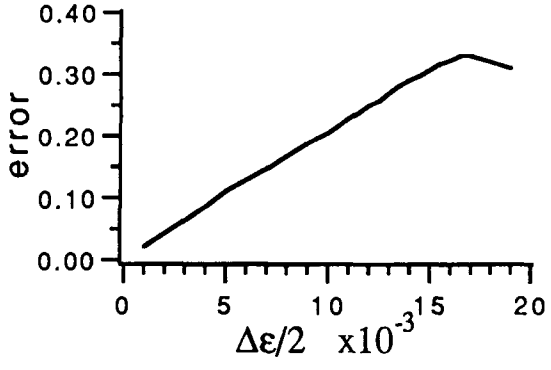

(c)

Fig. 3. a) Total useful diffraction efficiency η_T versus the modulation amplitude $\Delta\varepsilon/2$ of one primary grating for the corrected phases (solid line) and for the worst case (dashed line). b) Signal-to-noise ratio SNR and c) uniformity error e versus $\Delta\varepsilon/2$ for the corrected case. Recording parameters: λ = 0.514 μm, n = 1.5, B = 1, θ_0 = 45°, $\Delta\alpha$ = 1°, d = 15 μm.

The recording parameters for Tables 1-4 are: λ = 0.514 μm, n = 1.5, θ_0 = 45°, d = 15 μm.

$\Delta\alpha$ = 1°	$\Delta\varepsilon/2$	η_T	SNR	e
B = 1	0.0120	0.88	8.8	0.25
B = 2	0.012	0.93	16.8	0.19
B = 5	0.0125	0.97	31.4	0.12

Table 1. Results for 3 object beams with corrected phases. Modulation of the primary gratings $\Delta\varepsilon$, maximum useful diffraction efficiency η_{Tmax}, signal to noise ratio SNR, and uniformity error e as a function of the beam ratio B for an interbeam angle $\Delta\alpha$ = 1°.

$\Delta\alpha$ = 1°	$\Delta\varepsilon/2$	η_T	SNR	e
B = 1	0.0085	0.39	1.8	1.01
B = 5	0.0110	0.68	4.0	0.48
B = 10	0.0115	0.75	4.6	0.31
B = 20	0.0120	0.78	4.6	0.29

Table 2. Results for the worst case, i.e. 3 object beams in phase. Modulation of the primary gratings $\Delta\varepsilon$, maximum useful diffraction efficiency η_{Tmax}, signal to noise ratio SNR, and uniformity error e as a function of the beam ratio B for an interbeam angle $\Delta\alpha$ = 1°.

$\Delta\alpha = 0.1°$	$\Delta\varepsilon/2$	η_T	SNR	e
B = 1	0.0070	0.95	18.7	0.20

Table 3. Results for 9 object beams with corrected phases. Modulation of the primary gratings $\Delta\varepsilon$, maximum useful diffraction efficiency η_{Tmax}, signal to noise ratio SNR, and uniformity error e as a function of the beam ratio B for an interbeam angle $\Delta\alpha = 0.1°$.

$\Delta\alpha = 0.1°$	$\Delta\varepsilon/2$	η_T	SNR	e
B = 1	0.0050	0.09	0.2	2.89
B = 10	0.0070	0.20	0.7	1.90

Table 4. Results for the worst case, i.e. 9 object beams in phase. Modulation of the primary gratings $\Delta\varepsilon$, maximum useful diffraction efficiency η_{Tmax}, signal to noise ratio SNR, and uniformity error e as a function of the beam ratio B for an interbeam angle $\Delta\alpha = 0.1°$.

5. DISCUSSION

From the numerical results, we can see clearly the importance of using corrected phases for the object beams. For a reference-to-object beam ratio equal to unity, the fan-out element posses already good characteristics, even for the case of small angular separation: high total useful diffraction efficiency $\eta_{Tmax} \sim 95\%$ and relatively good uniformity $e < 0.2$ (see Table 3). Note, that at recording the N = 9 amplitudes of the object beams are equal $A_i = 1$. A perfect uniformity can be achieved, by adapting the amplitudes A_i or by copying an optimized uniform fan-out-element.

It is surprising, that for 9 object beams in phase the total useful diffraction efficiency reaches only 20%, even for a reference-to-object beam ratio equal to 10 (Table 4). This can be explained by unwanted cross coupling effects.

In the ideal case the Bragg condition is only fulfilled for the reconstruction of the desired N object waves through the primary gratings $\mathbf{K}_{0i}$. For fan-out elements neighboring beams are rather close, thus the interactions are still close to the Bragg condition. Cross coupling between the object waves (O-waves) and intermodulation waves (I-waves) through the thick and efficient gratings $\mathbf{K}_{0i}$ occur, as shown in Fig. 2. They are influenced by the phases Φ_{0i}, but not by the beam ratio. Note, that this interactions are also present for sequentially recorded holograms.

The influence of the cross coupling depends on the interbeam angle between two neighboring beams $\Delta\alpha = \alpha/(N - 1)$. If the phase mismatch becomes 2π, then the coupling is no longer efficient. For the arrangement shown in Fig. 1 these off-Bragg interactions are important for a hologram thickness t smaller than

$$t < \lambda/(n \tan\theta_0 \Delta\alpha), \tag{18}$$

where λ is the wavelength, θ_0 the reference beam angle, $\Delta\alpha = \alpha/(N - 1)$ the interbeam angle, and n the refractive index. As a consequence, for larger interbeam angle $\Delta\alpha$ and thicker holograms, the fan-out properties become less sensitive to the phases.

The intermodulation gratings $\mathbf{k}_{pq}$ are considered to be thin. Only a few percent of the light is exchanged by those gratings, but for the uniformity this is already too much. In the non-optimized case these gratings are added coherently, thereby magnifying its influence.

6. DYNAMIC RANGE

A holographic emulsion has a limited dynamic range, which depends on the material and the thickness. For an optimum hologram recording the exposure energy has to be within the dynamic range. If the exposure is increased above saturation, the emulsion will not generate a higher index modulation. For a high reference-to-object beam ratio and large fan-outs the limited dynamic range becomes important.

Figure 4 shows the interference pattern in the hologram plane (y-axis) of 9 object beams with a reference wave for a) optimized phases and b) worst case. We have assumed the same maximum modulation level and optimum contrast for the primary gratings. Whereas in the optimized case the beam ratio is B = 1, in the non-optimized case the beam ratio becomes B = 9.

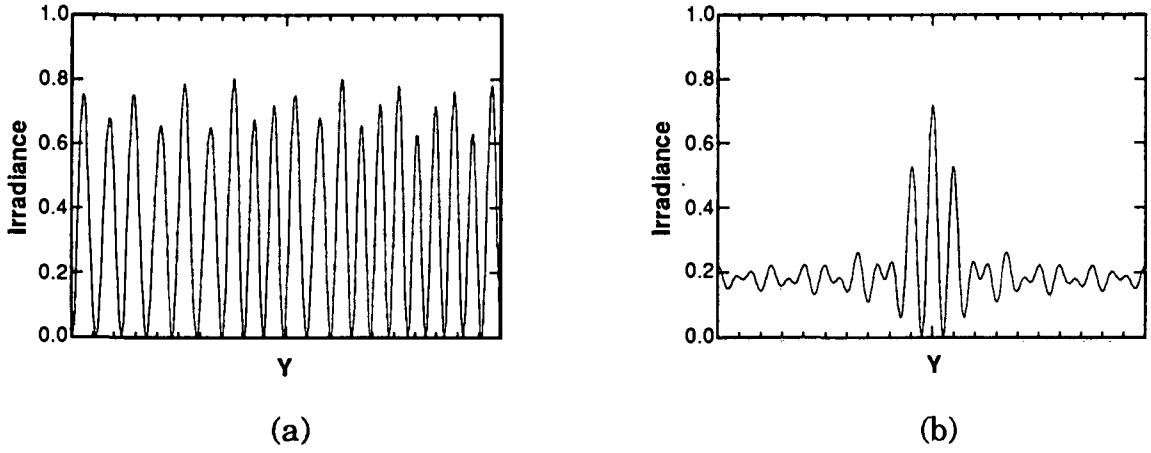

Fig. 4. Interference pattern in the hologram plane (y-axis) of 9 object beams with a reference wave for a) optimized phases, and b) worst case, for the same maximum modulation level.

We have compared the recording of one object wave with the recording of N object waves. In the optimized case, the exposure energy required for high efficiency becomes independent of N. In the non-optimized case, however, the same efficiency would require an exposure energy which is $\sqrt{N}$ times higher. The maximum fanout will then be limited by the saturation level.

7. RECORDING OF OPTIMIZED FAN-OUT ELEMENTS

Figure 5 shows the recording set-up for on-axis fanout elements. The object is an array of coherent sources with optimized phases ϕ_i. Such an array can be obtained by different techniques; e.g., using phase plates, CGH, kinoforms,[3] by copying Dammann gratings[2]. The hologram is placed in the far-field, i.e. in the Fourier plane of a lens. If the sources are in the front focal plane of the lens (d = f), the recorded element becomes non-focussing, and for larger object distances (d > f), it becomes focussing. Figure 6 shows the off-axis equivalent. Due to the limited depth of the optimum plane [Eq. (6)], source array and HOE have to be parallel.

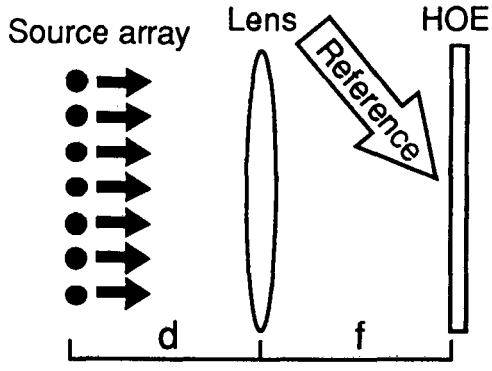

Fig. 5. Object waves on-axis, the HOE becomes focussing for $d > f$ and non-focussing for $d = f$.

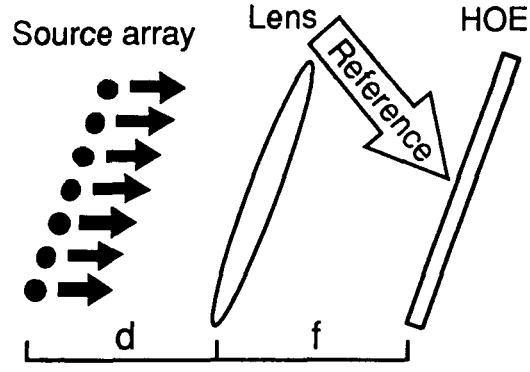

Fig. 6. Object waves off-axis.

8. CONCLUSIONS

We have investigated the recording of efficient fanout elements as volume holograms by using coupled wave theory. In opposition to the results published in the standard literature, we have found that the efficiency and uniformity of regular fanout elements depend strongly on the relative phases of the object waves, if the thickness t of the holographic emulsion is smaller than $t < \lambda/(n \tan\theta_0 \Delta\alpha)$, [Eq. (18)], e.g. $t < 32$ μm for $\lambda = 488$ nm, $n = 1.5$, $\theta_0 = 30°$ and $\Delta\alpha = 1°$. High efficiency and uniformity can be achieved by optimized phases of the object beams, thereby requiring a low dynamic range of the holographic material.

The recording conditions are optimum if the irradiance of the object beam is uniform in the hologram plane. This can be achieved only in specific planes, which are parallel to the object plane. As a consequence, only specific recording geometries are allowed.

9. REFERENCES

1. R. K. Kostuk, "Comparison of models for multiplexed holograms," Appl. Opt. **28**, 771-777 (1989).

2. B. Robertson, M. R. Taghizadeh, J. Turunen, A. Vasara, "High-efficiency, wide-bandwidth optical fanout elements in dichromated gelatin," Opt. Lett. **15**, 694-696 (1990).

3. H. P. Herzig, D. Prongué, R. Dändliker, "Design and fabrication of highly efficient fan-out elements," Jpn. J. Appl. Phys. **29**, L 1307-L 1309 (1990).

Fan-out elements recorded as volume holograms: optimized recording conditions

H. P. Herzig, P. Ehbets, D. Prongué, R. Dändliker

Institute of Microtechnology, University of Neuchâtel, Rue A.-L. Breguet 2, CH-2000 Neuchâtel, Switzerland

Abstract

The recording of efficient fan-out elements as volume holograms has been investigated by using coupled wave theory. In opposition to the results published in the standard literature, we have found that efficiency and uniformity of regular fan-out elements depend strongly on the relative phases of the object waves, at least if the thickness of the hologram is less than about 50 wavelengths. High efficiency and uniformity can be achieved by optimized recording conditions. At the same time the required dynamic range of the holographic material becomes minimum.

Key words: Fan-out element, coupled wave theory, volume hologram

Accepted for publication in Applied Optics, Vol. 31, 1992

1. Introduction

Optical fan-out elements divide a single laser beam into a regular array of equally intense light spots in one- or two-dimensions. They are used in many applications of modern optics, such as parallel optical processing and fiber optic communication. Today, fan-out elements are fabricated synthetically as surface-relief phase structure by using microfabrication techniques (e.g. [1], section 6). Such elements are Dammann gratings [2], multilevel gratings [3], or continuous surface relief structures [4]. However, proper modulation at large carrier frequencies (> 1000 lines/mm) is difficult to achieve by mask projection. Therefore, interferometrically recorded holograms are still of interest for realizing off-axis elements and large fan-out numbers. This paper deals with the recording of efficient fan-out elements in thick volume holograms. We have applied coupled wave theory to study the recording conditions for high diffraction efficiency and uniformity of the generated array of beams.

Papers about coupled wave theory for multiple beam recording predict high efficiency for replaying N waves and only weak dependence of interactions between the beams, because of the highly selective Bragg condition [5]. This would suggest that the recording of fan-out elements is an easy task. However, experimental results show the difficulties for recording uniform fan-out elements as volume holograms and the precaution necessary to generate a uniform distribution of the irradiance in the hologram plane [6]. The fundamental difficulties are explained in terms of recording non-linearity. Using coupled wave theory, we have found that also for perfect linearity the hologram does not generate a uniform fan-out [7]. We shall demonstrate how to apply coupled wave theory to the special problem of regular fan-out elements. These elements are called degenerated, because all gratings with equal periodicity diffract light in the same direction and must be added coherently. As a consequence, the

results for efficiency and uniformity depend strongly on the relative phases of the recorded object waves.

2. Simultaneous recording with minimum intermodulations

A fan-out element can be fabricated by recording a hologram of N object waves $E_i(\mathbf{x}) = A_i \exp\{-j\mathbf{k}_i\cdot\mathbf{x} + j\phi_i\}$ with a reference wave $E_0(\mathbf{x}) = A_0 \exp\{-j\mathbf{k}_0\cdot\mathbf{x} + j\phi_0\}$. The basic configuration is shown in Fig. 1. The waves are characterized by the wavevectors $\mathbf{k}_i = (k_i^y, k_i^z)$, amplitudes A_i, and phases ϕ_i, where $\mathbf{x} = (y,z)$ are the coordinates. Only the s polarization is considered.

We assume, that the recording material responds linearly to the accumulated energy during exposure, i.e.

$$\varepsilon(y,z) = \varepsilon_a + \delta \left| \sum_{i=1}^{N} E_i + E_0 \right|^2 . \tag{1}$$

The dielectric permittivity $\varepsilon(y,z)$ after exposure becomes then

$$\varepsilon(y,z) = \varepsilon_a' + \sum_{i=1}^{N} \Delta\varepsilon_{0i}\cos(\mathbf{K}_{0i}\cdot\mathbf{x} - \Phi_{0i}) + \sum_{q>p=1}^{N} \Delta\varepsilon_{pq}\cos(\mathbf{K}_{pq}\cdot\mathbf{x} - \Phi_{pq}), \tag{2}$$

where $\Phi_{pq} = \phi_p - \phi_q$ and $\Delta\varepsilon_{pq} = 2\delta A_p A_q$. Besides the desired N primary gratings $\mathbf{K}_{0i} = \mathbf{k}_0 - \mathbf{k}_i$, $N(N-1)/2$ unwanted intermodulation gratings $\mathbf{K}_{pq} = \mathbf{k}_p - \mathbf{k}_q$ are recorded. At readout, they generate intermodulation waves, which are coupled with the desired reconstructed beams. As a consequence, efficiency and uniformity of the fan-out suffer.

One possibility to reduce the intermodulations with respect to the primary gratings is to increase the reference-to-object beam ratio B [5], which is defined by

$$B = \frac{A_0^2}{\sum_{i=1}^{N} A_i^2} . \qquad (3)$$

Then, the modulations of the desired primary gratings become dominant ($\Delta\varepsilon_{0i} >> \Delta\varepsilon_{pq}$). Unfortunately this method requires a very high dynamic range of the recording material.

It has been shown earlier, that for on-axis regular fan-out elements the intermodulation gratings can be eliminated nearly perfectly [4]. In the case of regular elements, the projections $K_{pq}^{\ y}$ of the grating vector $\mathbf{K}_{pq}$ in the hologram plane (y-axis) are all integer multiples of the lowest frequency $2\pi\nu$ formed by the interference between two neighboring object beams. Thus, we can write the intermodulation term in Eq. (2) as

$$\sum_{q>p}^{N} \Delta\varepsilon_{pq} \cos(\mathbf{K}_{pq}\cdot\mathbf{x} - \Phi_{pq}) = \sum_{q>p}^{N} \Delta\varepsilon_{pq} \cos(2\pi m\nu y + K_{pq}^{\ z} z - \Phi_{pq}), \qquad (4)$$

where $m = p - q$. There are $N - 1$ gratings with $m = 1$, $N - 2$ gratings with $m = 2$, etc. By adding the gratings with the same frequency, but optimized phase shifts Φ_{pq}, one can minimize the intermodulations [4]. Note, that the grating with the highest frequency ($m = N - 1$) cannot be cancelledd, because it appears only once.

The intermodulations vary in the z-direction with $K_{pq}^{\ z}$ [Eq. (4)]. As a consequence they can be minimized only for one specific plane parallel to the hologram plane ($z = \text{const}$). For on-axis object beams, as shown in Fig. 1, the z-variation is rather slow, i.e. $K_{pq}^{\ z}$ is small. The largest component $K_{pq}^{\ z}$ is formed by the interference between the central beam, propagating in the direction of the z-axis, and the marginal beams of the fan-out. We obtain

$$(K_{pq}^{\ z})_{max} = \frac{2\pi}{\lambda} n(1 - \cos\frac{\alpha}{2}) = \frac{2\pi}{\Lambda} , \qquad (5)$$

where λ is the wavelength, α the full angle $(\mathbf{k}_1,\mathbf{k}_N)$ of the fan-out, n the refractive index, and Λ the periodicity of the grating $(K_{pq}{}^z)_{max}$. The intermodulations remain small within a depth h of $\pm \Lambda/10$, i.e.

$$h = \frac{\Lambda}{5} = \frac{\lambda}{5n(1 - \cos(\alpha/2))} \quad . \tag{6}$$

We can conclude, that for the geometry shown in Fig. 1 the hologram plane must be normal to the z-axis, within the tolerances given by Eq. (6). This restricts the optimum recording geometry.

For very thick holograms the off-Bragg interactions become negligible and therefore the phases of the object waves are irrelevant. In this case the recording geometry is not restricted by Eq. (6).

3. Coupled wave equations

In the following, we shall derive the coupled wave equations for regular fan-out elements. The electrical field has to fulfill the Helmholtz equation

$$\Delta E(y,z) + k^2 \varepsilon(y,z) E(y,z) = 0, \tag{7}$$

with $k = (2\pi/\lambda)$ and $\varepsilon(y,z)$ as determined by Eq. (2).

The total electric field inside the hologram is written as a sum of M plane waves diffracted in different directions

$$E(y,z) = E_0(y,z) + \sum_{i=1}^{N} E_i(y,z) + \sum_{i=N+1}^{M} E_i(y,z) \ , \tag{8}$$

where the first N waves are the desired object waves. Each component of the electric field is of the form

$$E_i(y,z) = B_i(z)\,\exp\{-j\mathbf{k}_i\cdot\mathbf{x}\}, \tag{9}$$

where $B_i(z)$ are complex amplitudes.

The waves $E_i(y,z)$ are generated by diffraction of an incident beam ($\mathbf{k}_m$) at a grating $\mathbf{K}_{pq}$. The wavevectors $\mathbf{k}_i$ are then determined by the beta-value construction, namely

$$k_i^y = k_m^y - K_{pq}^y, \qquad q > p = 0,...,N-1;\;\; i,m = 0,...,M. \tag{10}$$

For the z-components we obtain

$$k_i^z = \sqrt{k^2\varepsilon_a - (k_i^y)^2}\,. \tag{11}$$

The coupled wave equations are now obtained by introducing the electrical field [Eq. (8)], into the Helmholtz equation (7). This yields

$$\frac{dC_m}{dz}\cos\theta_m = -j\sum_{n=0}^{M} W_{mn}\,C_n, \qquad m = 0,...,M, \tag{12}$$

where $C_i = B_i\exp\{-jk_i^z z\}$. The reason for this substitution is to separate the wave parameters, described by the coefficients C_i, and the independent grating parameters, described by the matrix W_{mn}. Note, that the matrix must be hermitian, i.e. $W_{mn} = W_{nm}^*$, and that the diagonal elements are equal to zero, i.e. $W_{mm} = 0$.

For a simple coupling between two waves E_m and E_n through one grating $\mathbf{K}_{pq}$, we get

$$W_{mn} = \chi_{pq} = \kappa_{pq}\exp\{j(-K_{pq}^z z) + \Phi_{pq})\}. \tag{13}$$

$\kappa_{pq} = k\Delta\varepsilon_{pq}/4$ is Kogelnik's coupling coefficient for the grating $\mathbf{K}_{pq}$.

We have to consider that each beam E_m diffracts at all gratings. In our degenerated case all gratings with equal periodicity, i.e. equal K_{pq}^y, diffract light in the same direction. Their coupling coefficients have to be added coherently, which means

$$W_{mn} = \sum \chi_{pq} , \qquad \text{for } q - p = \text{const.} \qquad (14)$$

Figure 2 shows the spectrum of the waves included in our model for a fan-out of N = 3 and possible interactions for object wave (O-wave) no. 2 through the three primary gratings $\mathbf{K}_{01}$, $\mathbf{K}_{02}$, $\mathbf{K}_{03}$ and the three intermodulation gratings $\mathbf{K}_{12}$, $\mathbf{K}_{23}$, $\mathbf{K}_{13}$. For further reading, I-waves are the intermodulation waves generated by diffraction of the readout wave at the intermodulation gratings $\mathbf{K}_{pq}$, and S-waves are the secondary waves generated by diffraction of the object waves at the intermodulation gratings $\mathbf{K}_{pq}$.

For a fan-out of N waves, we have made the following assumptions for our coupled wave model:

- Simultaneous recording of N object waves and one reference wave leads to N primary gratings $\mathbf{K}_{0i}$ and N(N – 1)/2 intermodulation gratings $\mathbf{K}_{pq}$, where q > p = 1,...,(N – 1).
- The primary gratings are thick, only one diffraction order is considered.
- The intermodulation gratings are considered to be optically thin, the ± first diffraction orders are included.
- At readout, N object waves (O-waves), 2(N – 1) secondary waves (S-waves) and 2(N – 1) intermodulation waves (I-waves) are generated.
- Any possible coupling between the waves E_m through the gratings $\mathbf{K}_{0i}$ and $\mathbf{K}_{pq}$ are accepted.
- Coupling coefficients χ_{pq} of gratings with equal periodicity, i.e. equal K_{pq}^{y}, are added coherently.

4. Numerical results

The coupled wave equations (12) have been solved by numerical integration using Runge-Kutta. The boundary conditions for transmission holograms at z = 0 are: $C_0 = 1$ and $C_i = 0$ for i = 1,...,M.

The diffraction efficiency η_T of all object waves is obtained from Eq. (15):

$$\eta_T = \sum_{i=1}^{N} \eta_i \qquad \text{with} \qquad \eta_i = \frac{\cos\theta_i}{\cos\theta_0} |C_i|^2, \quad i = 1,...,N. \tag{15}$$

Important for fan-out elements is the uniformity error e described by

$$e = \frac{\eta_{i_{max}} - \eta_{j_{min}}}{< \eta_i >} . \tag{16}$$

In the following, we distinguish between the corrected and the uncorrected case. The corrected case has optimized phases Φ_{pq} for minimum intermodulations at the point z = 0, i.e. at the surface of the holographic emulsion. Except in the trivial case of 3 waves, the phases Φ_{pq} have been determined by numerical optimization [4]. In the uncorrected, worst case, a constant phase is assumed. We have calculated the results for a fan-out of N = 3 (Fig. 3 and Table 1) and N = 9 (Fig. 4 and Table 2). The following values have been used for the calculations:

- For 3 object beams: $\phi_1 = \phi_3 = 0$, $\phi_2 = \pi/2$.
- For 9 object beams: $\phi_1 = \phi_9 = 1.77219$, $\phi_2 = \phi_8 = 0.13512$, $\phi_3 = \phi_7 = 3.88710$, $\phi_4 = \phi_6 = 2.45465$, $\phi_5 = 3.14159$ rad.
- Uncorrected, worst case: $\phi_i = 0$.

Note, that $\Phi_{pq} = \phi_p - \phi_q$.

Figures 3 and 4 show the total useful diffraction efficiency η_T and the uniformity error e as a function of the modulation amplitude $\Delta\varepsilon = \Delta\varepsilon_{0i}$ of one primary grating for N = 3

and N = 9, respectively. The corrected cases (solid line) show a high diffraction efficiency and a good uniformity. The efficiency increases up to a maximum with increasing modulation, similar to the behavior of a single grating in a volume hologram. In the uncorrected cases (dashed line), the efficiency is low and the uniformity is poor. Note, that the modulation amplitude $\Delta\varepsilon$ necessary for optimum efficiency is about $\sqrt{N}$ smaller than in the case of a single grating.

The angular separation of the fan-out is indicated by the angle $\Delta\alpha = \theta_{i+1} - \theta_i$ between two neighboring object beams. Tables 1 and 2 present the maximum diffraction efficiency η_T for different interbeam angles $\Delta\alpha$ and different beam ratios B, again for N = 3 and N = 9, respectively. From the numerical results we can see clearly the importance of using corrected phases for the object beams. For a reference-to-object beam ratio equal to unity, the fan-out element posses already good characteristics. For example, for N = 9 and $\Delta\alpha = 0.1°$ the maximum diffraction efficiency becomes $\eta_{Tmax} \sim 94\%$ with a relatively good uniformity of $e < 0.2$.

All calculations have been made with the following parameters: wavelength $\lambda = 0.488\ \mu m$, refractive index of the holographic medium n = 1.5, thickness of the medium $d = 15\ \mu m$, and reference beam angle $\theta_0 = 30°$.

5. Discussion

In this chapter, we try to explain the results obtained by our coupled wave model. We have found that for small interbeam angles $\Delta\alpha$ the corrected phases give a much better efficiency. For larger angles the effect is less significant. A similar behavior is observed for the uniformity error e, except that for large $\Delta\alpha$ the uniformity may become bad.

In the ideal case, the Bragg condition is only fulfilled for the reconstruction of the desired N object waves through the primary gratings $\mathbf{K}_{0i}$. In reality, also unwanted cross coupling between the object waves (O-waves) and intermodulation waves (I-waves) through the efficient gratings $\mathbf{K}_{0i}$ occur, as shown in Fig. 2. These interactions are influenced by the phases Φ_{0i}, but not by the beam ratio B (see results for $\Delta\alpha = 0.1°$). For fan-out elements neighboring beams are rather close, thus the interactions are still close to the Bragg condition. Figure 5 shows the typical off-Bragg behavior of a thick volume grating. We assume, that wave i fulfils the Bragg condition. It has been generated by diffraction at the grating $\mathbf{K}_{0i}$. The neighboring wave i+1 can also receive light through the same grating $\mathbf{K}_{0i}$, but this interaction is now off-Bragg. The coupling remains efficient, if the phase mismatch is less than 2π. We have applied this criterion to the arrangement shown in Fig. 1. It turns out, that these off-Bragg interactions are important for a hologram thickness smaller than

$$t = \lambda/(n \tan\theta_0 \Delta\alpha), \tag{18}$$

where $\Delta\alpha = \alpha/(N-1)$ is the interbeam angle between two neighboring beams, θ_0 the reference beam angle, λ the wavelength, and n the refractive index. As a consequence, for larger interbeam angle $\Delta\alpha$ and thicker holograms, the fan-out properties become less sensitive to the phases. This can be observed for the efficiencies but not for the uniformities.

We have assumed, that at recording the N amplitudes of the object beams are equal $A_i = 1$. For small interbeam angles $\Delta\alpha$, a perfect uniformity ($e < 0.01$) has been achieved by adjusting the amplitudes A_i.

There are different reasons for uniformity errors. One reason is that the coupling coefficients depend on the directions of the wave propagation. Another reason is that, also for optimized phases, the intermodulation gratings $\mathbf{K}_{pq}$ are only canceled within a

depth h given by Eq. (6). For larger fan-out angles α, the depth h becomes very short and therefore undesired intermodulation gratings are recorded. As a result the uniformity error increases as observed for $\Delta\alpha = 5°$, i.e. $\alpha = 10°$ (Table 1) and $\Delta\alpha = 3°$, i.e. $\alpha = 24°$ (Table 2). This error can be reduced by the beam ratio B or by the position of the plane of minimum intermodulations. As already mentioned earlier, the corrected case has optimized phases Φ_{pq} for minimum intermodulations at the point $z = 0$, i.e. at the surface of the holographic emulsion. If we place the plane with minimum intermodulation in the center of the hologram at $z = d/2$, the uniformity error decreases significantly (see * in Tabels 1 and 2).

The uniformity problems observed for large angles between the beams are created by the thin intermodulation gratings $\mathbf{K}_{pq}$. We think that this gratings are not sufficiently described in our model by taking into account only the ±1st orders. A more rigorous theory is necessary to treat them exactly also for large angles.

Note, that for sequentially recorded holograms the intermodulation gratings $\mathbf{K}_{pq}$ are not recorded, whereas the strong cross coupling through primary gratings $\mathbf{K}_{0i}$ is also present.

6. Dynamic range

A holographic emulsion has a limited dynamic range, which depends on the material and the thickness. For an optimum hologram recording the exposure energy has to be within the dynamic range. If the exposure is increased above saturation, the emulsion will not generate a higher index modulation. For a high reference-to-object beam ratio and large fan-outs the limited dynamic range becomes important. We will show, that recording with optimized phases requires a lower dynamic range.

At recording, N object waves $E_i(\mathbf{x}) = A \exp\{-j(\mathbf{k}_i \cdot \mathbf{x} + \phi_i)\}$ and one reference wave $E_0(\mathbf{x}) = A_0 \exp\{-j(\mathbf{k}_0 \cdot \mathbf{x} + \phi_0)\}$ are present. As shown in Eq. (1), the irradiance $I(\mathbf{x})$ in the hologram plane is given by

$$I(\mathbf{x}) = \left| \sum_{i=1}^{N} E_i + E_0 \right|^2 \tag{19}$$

$$= A_0^2 + NA^2 + 2A_0A \sum_{i=1}^{N} \cos(\mathbf{K}_{0i} \cdot \mathbf{x} - \Phi_{0i}) + 2A^2 \sum_{q>p=1}^{N} \cos(\mathbf{K}_{pq} \cdot \mathbf{x} - \Phi_{pq}),$$

with $\Phi_{pq} = \phi_p - \phi_q$ and $\mathbf{K}_{pq} = \mathbf{k}_p - \mathbf{k}_q$.

Figure 6 shows the irradiance $I(\mathbf{x})$ in the hologram plane (y-axis) for optimized phases and for the worst case ($\Phi_{0i} = \Phi_{pq} = 0$), respectively. Both cases are calculated for maximum contrast, i.e. $I_{min} = 0$, and for the same maximum irradiance I_{max}. In the uncorrected case ($\Phi_{0i} = \Phi_{pq} = 0$), all gratings are in phase at $x = 0$ and $y = 0$, thus all amplitudes add up and produce a high maximum intensity. In the corrected case with the optimized phases, however, the primary gratings $\mathbf{K}_{0i}$ are never all in phase at the same position and the intermodulation term, containing the gratings $\mathbf{K}_{pq}$, disappears nearly perfectly. Then, the first summation in Eq. (19) yields $2A_0A\sqrt{N}$ and the second summation, i.e. the intermodulations, can be omitted. The maximum and minimum values of the irradiance are found to be

$$I_{max} = (A_0 + \sqrt{N}A)^2, \qquad I_{min} = (A_0 - \sqrt{N}A)^2 \tag{20}$$

for the corrected case and

$$I_{max} = (A_0 + NA)^2, \qquad I_{min} = (A_0 - NA)^2 \tag{21}$$

for the uncorrected case, where N is the number of fan-out beams and A is the amplitude of the object waves for the recording. Maximum contrast is obtained for $I_{min} = 0$, which gives the relations $A_0 = \sqrt{N}A$ and $A_0 = NA$ for the two cases,

respectively. We get then from Eq. (3) a reference-to-object ratio of B = 1 for the optimized phases, whereas for the uncorrected case B = N, which means that the corrected case requires considerably less reference irradiance.

The modulation of the dielectric permittivity $\Delta\varepsilon_{0i}$ for the primary gratings $\mathbf{K}_{0i}$, as shown in Eq. (2), is proportional to $2A_0A$. Assuming that the recording material saturates at a level corresponding to an irradiance of $I_{max} = I_s$, we find then from Eqs. (20) and (21) with $I_{min} = 0$

$$\Delta\varepsilon_{0i} \propto 2A_0A = 2\sqrt{N}A^2 = I_s/2\sqrt{N} \tag{22}$$

for the corrected case and

$$\Delta\varepsilon_{0i} \propto 2A_0A = 2NA^2 = I_s/2N \tag{23}$$

for the uncorrected case, which means that the recorded modulation $\Delta\varepsilon_{0i}$ for the primary gratings is $\sqrt{N}$ times higher for the optimized phases. Besides the fact that the fan-out is more efficient in the case of corrected phases, as shown in Figs. 3 and 4, the required modulation amplitude $\Delta\varepsilon$ for maximum efficiency can be obtained easier within the limited dynamic range of the recording material.

7. Recording optimized fan-out elements

Figure 7(a) shows the recording set-up for on-axis fan-out holograms. The object is an array of coherent sources. The optimized phases ϕ_i can be obtained by different techniques. One possibility is to illuminate a pinhole array followed by an appropriate phase plate, another is to use CGHs, or kinoforms (see Figs. 6 and 7 in Ref. 4). The hologram is placed in the far-field, i.e. in the Fourier plane of a lens. If the sources are in the front focal plane of the lens (d = f), the recorded element is non-focussing, for larger object distances (d > f) it becomes focussing. Figure 7(b) shows the off-axis

equivalent. Due to the limited depth of the optimum plane [Eq. (6)], source array and HOE have to be parallel.

If the lens is removed, we get a focussing fan-out element. However, the optimized phases will generate a uniform illumination only if the hologram is in the far-field, i.e. at a distance $d > (Ns)^2/\lambda$, see Fig. 8(a). Another method to fabricate focussing fan-out elements without a lens uses the self-imaging properties of large periodic structures [8]. In this case the object is a regular array of coherent sources with identical phases $\phi_i = 0$. Considering the beam propagation in free space, planes of reduced intermodulations are found, which are suitable for recording efficient holograms. These planes are parallel to the object plane, as in the case of optimized phases. In Fig. 8(b) we incline the object, thus, we have also to incline the hologram. The self-imaging (Talbot) distance is proportional to s^2 and for inclined objects proportional to $(s\cos\theta)^2$. If we incline a regularly spaced 2-D array (same spacing s in x and y direction) with respect to the y-axis, we get two different distances for the optimum planes, depending on s^2 and $(s\cos\theta)^2$ respectively. However, a common minimum plane can be determined. This problem can be avoided if the initial array has two different periods Λ in the x and the y direction, namely $\Lambda_x = s$ and $\Lambda_y = s/\cos\theta$.

Due to the self-imaging properties, this method is only suitable for very large arrays. Note, that depending on the position of the recording plane, this element becomes either a fan-out (overlapping) or a lenslet array (non-overlapping beams).

Fan-out elements in volume holograms can also be fabricated by copying the phase structure of already existing fan-out element as e.g. Dammann gratings. A simple image formation with a single lens would destroy the phase structure and therefore the properties of the fan-out. This can be avoided by using a 4-f imaging system as shown in Fig. 9, which applies twice a Fourier transform thereby conserving the phase

distribution [6]. Analog to Figs. 7 and 8, there exists also an off-axis arrangement of Fig. 9.

8. Conclusions

We have investigated the recording of efficient fan-out elements as volume holograms by using coupled wave theory. In opposition to the results published in the standard literature, we have found that the efficiency and uniformity of regularly fan-out elements depend strongly on the relative phases of the object waves, if the thickness of the holographic emulsion is smaller than $t = \lambda/(n \tan\theta_0 \Delta\alpha)$, where θ_0 is the angle of the reference wave and $\Delta\alpha$ the angle between the fan-out beams. A typical value is $t = 32\ \mu m$ for $\lambda = 488$ nm, $n = 1.5$, $\theta_0 = 30°$ and $\Delta\alpha = 1°$. High efficiency and uniformity can be achieved by optimized phases of the object beams, which minimize the intermodulations. At the same time the required dynamic range of the holographic material becomes also minimum.

The recording conditions are optimum if the irradiance of the object beam is uniform in the hologram plane. This can be achieved only in specific planes, which are parallel to the object plane. As a consequence, only specific recording geometries are allowed. Several possible recording techniques to fabricate efficient and uniform fan-out elements have been presented.

9. References

[1] H. P. Herzig, R. Dändliker, "Holographic optical elements for use with semiconductor lasers," contribution to "International trends in optics," J. W. Goodman, ed., (Academic Press, New York, 1991) pp. 57-75.

[2] H. Dammann, K. Görtler, "High-efficiency in-line multiple imaging by means of multiple phase holograms," Opt. Commun. **3**, 312-315 (1971).

[3] S. J. Walker, J. Jahns, "Array generation with multilevel phase gratings," J. Opt. Soc. Am. A. **7**, 1509-1513 (1990).

[4] H. P. Herzig, D. Prongué, R. Dändliker, "Design and fabrication of highly efficient fan-out elements," Jpn. J. Appl. Phys. **29**, L 1307-L 1309 (1990).

[5] R. K. Kostuk, "Comparison of models for multiplexed holograms," Appl. Opt. **28**, 771-777 (1989).

[6] B. Robertson, M. R. Taghizadeh, J. Turunen, A. Vasara, "High-efficiency, wide-bandwidth optical fanout elements in dichromated gelatin," Opt. Lett. **15**, 694-696 (1990).

[7] H. P. Herzig, P. Ehbets, D. Prongué, R. Dändliker, "Fan-out elements by multiple beam recording in volume holograms," Proc. Soc. Photo-Opt. Instrum. Eng. **1507**, 247-255 (1991).

[8] I. Seyd-Darwish, P. Chavel, J. Taboury, Y. Malet, "Array illuminator hologram based on the Talbot effect," Conference Record of 1990 International Topical Meeting on Optical Computing, Kobe, 294-296 (April, 1990).

Figure captions

Fig. 1. (a) Recording and (b) readout of fan-out elements. The angles are defined inside the recording medium with refractive index $n = \sqrt{\varepsilon_a}$ (see Eq. 1), α is the full fan-out angle.

Fig. 2. Spectrum of the waves included in our model for a fan-out of N = 3 and possible interactions for object wave (O-wave) no. 2 through primary gratings $\mathbf{K}_{0i}$ and intermodulation gratings $\mathbf{K}_{pq}$.

Fig. 3. Results for a fan-out of **N = 3.** (a) Total useful diffraction efficiency η_T versus the modulation amplitude $\Delta\varepsilon$. The solid line corresponds to the case of corrected phases, the dashed line corresponds to the worst case. (b) Uniformity error e versus $\Delta\varepsilon$. Recording parameters: λ = 0.488 μm, n = 1.5, B = 1, $\theta_0 = 30°$, $\Delta\alpha = 1°$, d = 15 μm.

Fig. 4. Results for a fan-out of **N = 9.** (a) Total useful diffraction efficiency η_T versus the modulation amplitude $\Delta\varepsilon$. The solid line corresponds to the case of corrected phases, the dashed line corresponds to the worst case. (b) Uniformity error e versus $\Delta\varepsilon$. Recording parameters: λ = 0.488 μm, n = 1.5, B = 1, $\theta_0 = 30°$, $\Delta\alpha = 0.1°$, d = 15 μm.

Fig. 5. Wave i fulfils the Bragg condition when diffracted at the grating $\mathbf{K}_{0i}$, whereas wave $\mathbf{K}_{i+1}$ is off-Bragg. If the phase mismatch becomes 2π, the coupling is no longer efficient.

Fig. 6. Interference pattern in the hologram plane (y-axis) of 9 object beams with a reference wave for (a) optimized phases, and (b) worst case, for the same maximum modulation level.

Fig. 7. Object waves (a) on-axis and (b) off-axis; the HOE becomes focussing for $d > f$ and non-focussing for $d = f$.

Fig. 8. Recording without lens with spherical object waves (a) on-axis and (b) off-axis by using the self-imaging properties of large periodic structures.

Fig. 9. 4f-system for copying fan-out elements with magnification $m = f_2/f_1$, where $d = f_2$. Focussing power can be included if $d > f_2$.

Table captions

Table 1. Results for a fan-out of **N = 3.** Maximum useful diffraction efficiency η_T, uniformity error e, and modulation $\Delta\varepsilon$, for different beam ratios B and interbeam angles $\Delta\alpha$. Recording parameters: λ = 0.488 μm, n = 1.5, θ_0 = 30°, d = 15 μm (* see section 5. Discussion).

Table 2. Results for a fan-out of **N = 9.** Maximum useful diffraction efficiency η_T, uniformity error e, and modulation $\Delta\varepsilon$, for different beam ratios B and interbeam angles $\Delta\alpha$. Recording parameters: λ = 0.488 μm, n = 1.5, θ_0 = 30°, d = 15 μm (* see section 5. Discussion).

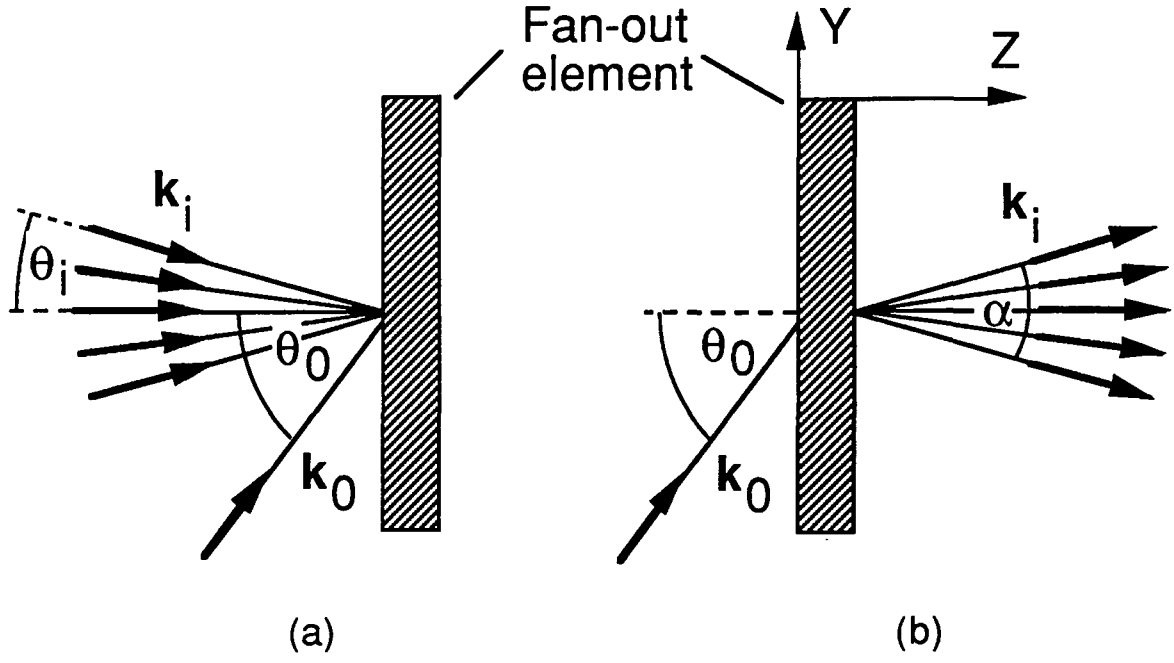

Fig. 1. (a) Recording and (b) readout of fan-out elements. The angles are defined inside the recording medium with refractive index $n = \sqrt{\varepsilon_a}$ (see Eq. 1), α is the full fan-out angle.

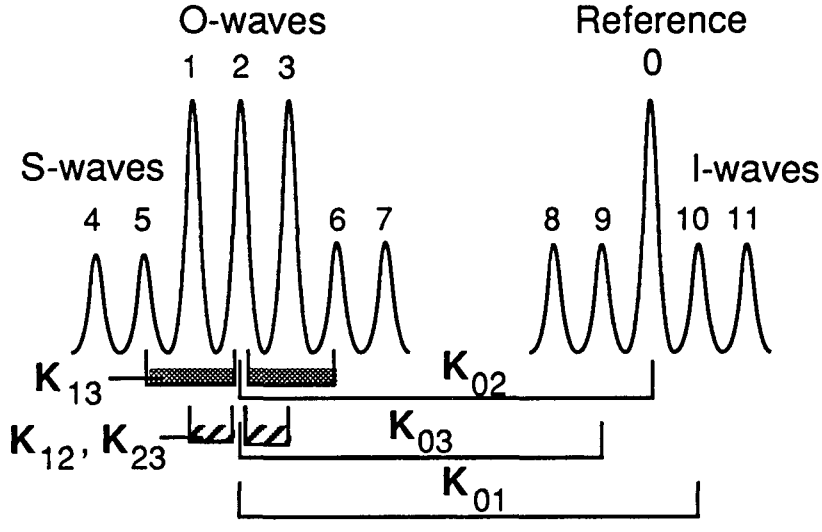

Fig. 2. Spectrum of the waves included in our model for a fan-out of N = 3 and possible interactions for object wave (O-wave) no. 2 through primary gratings K_{0i} and intermodulation gratings K_{pq}.

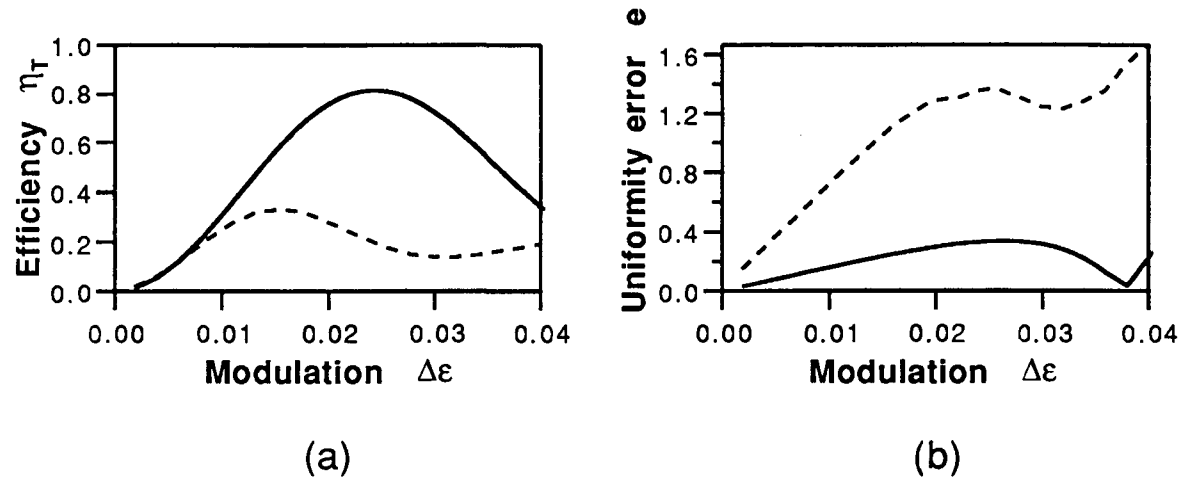

(a) (b)

Fig. 3. Results for a fan-out of **N = 3.** (a) Total useful diffraction efficiency η_T versus the modulation amplitude $\Delta\varepsilon$. The solid line corresponds to the case of corrected phases, the dashed line corresponds to the worst case. (b) Uniformity error e versus $\Delta\varepsilon$. Recording parameters: $\lambda = 0.488$ μm, n = 1.5, B = 1, $\theta_0 = 30°$, $\Delta\alpha = 1°$, d = 15 μm.

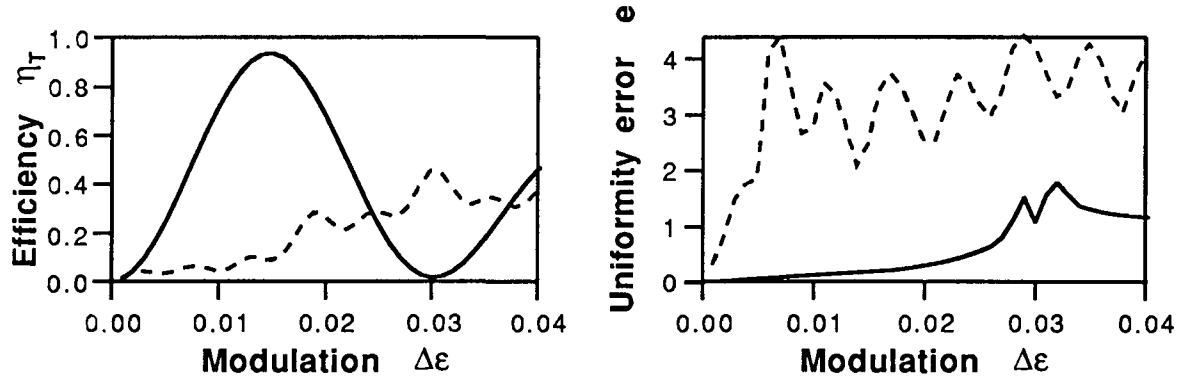

(a) (b)

Fig. 4. Results for a fan-out of **N = 9.** (a) Total useful diffraction efficiency η_T versus the modulation amplitude $\Delta\varepsilon$. The solid line corresponds to the case of corrected phases, the dashed line corresponds to the worst case. (b) Uniformity error e versus $\Delta\varepsilon$. Recording parameters: $\lambda = 0.488$ μm, n = 1.5, B = 1, $\theta_0 = 30°$, $\Delta\alpha = 0.1°$, d = 15 μm.

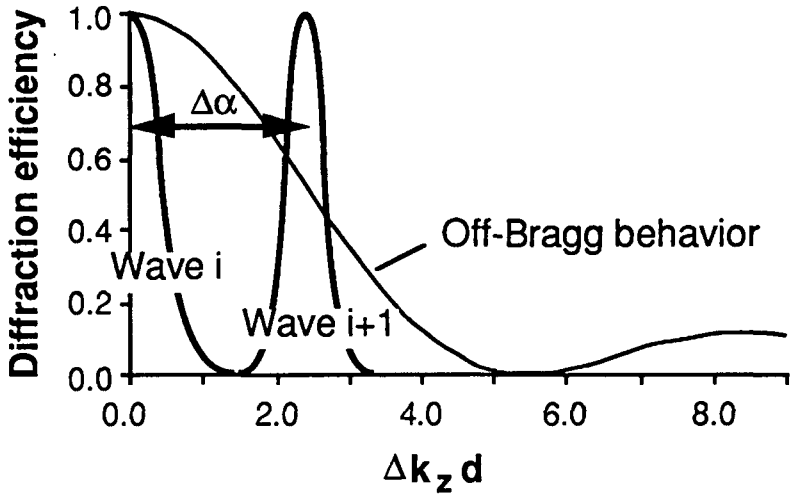

Fig. 5. Wave i fulfils the Bragg condition when diffracted at the grating K_{0i}, whereas wave K_{i+1} is off-Bragg. If the phase mismatch becomes 2π, the coupling is no longer efficient.

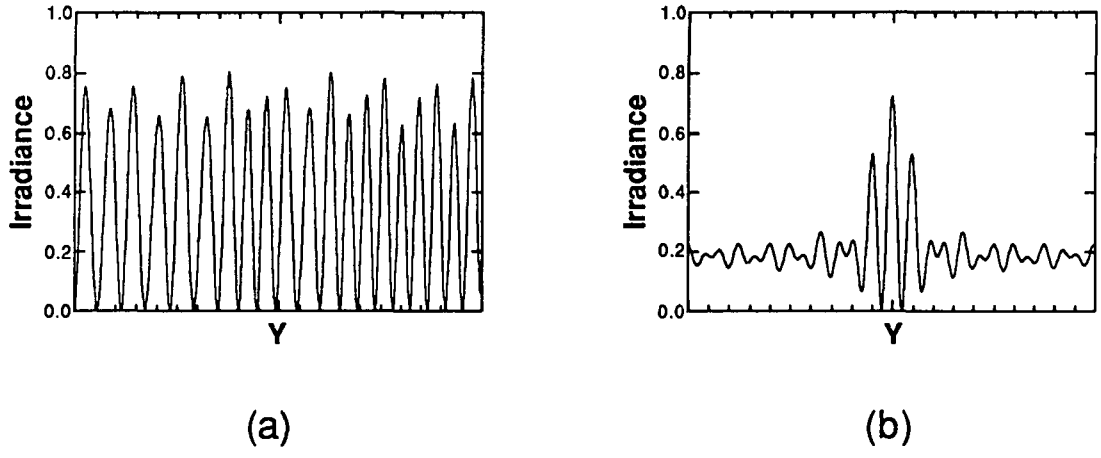

Fig. 6. Interference pattern in the hologram plane (y-axis) of 9 object beams with a reference wave for (a) optimized phases, and (b) worst case, for the same maximum modulation level.

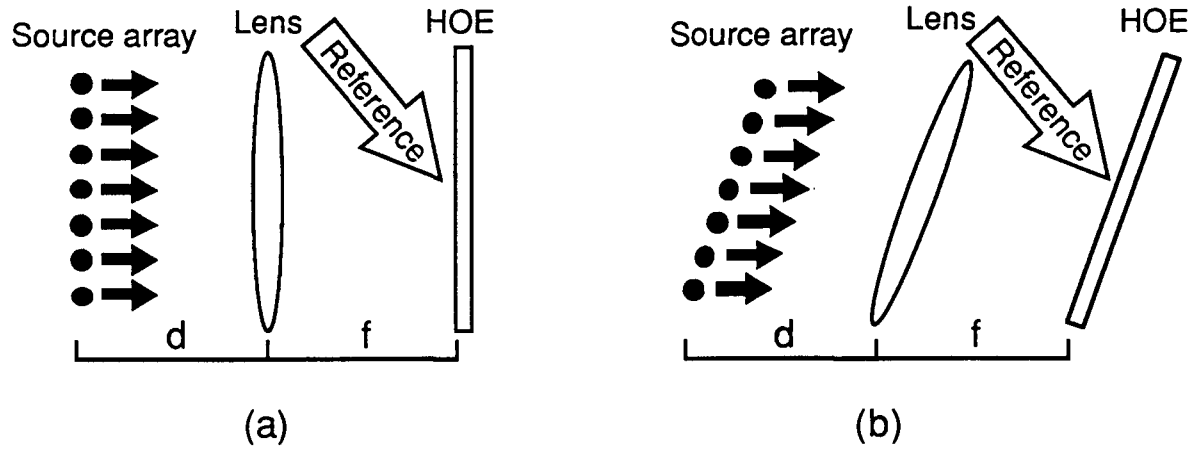

Fig. 7. Object waves (a) on-axis and (b) off-axis; the HOE becomes focussing for d > f and non-focussing for d = f.

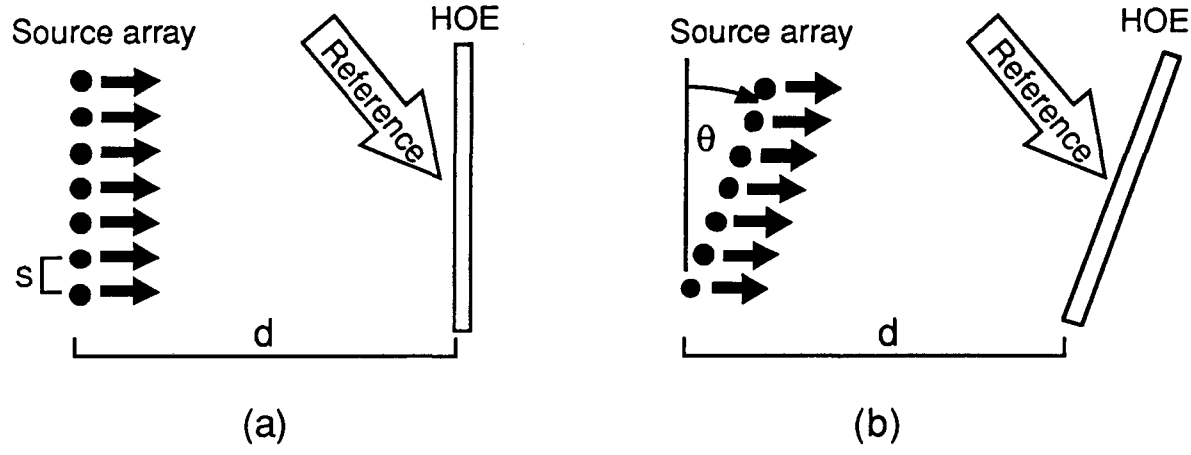

Fig. 8. Recording without lens with spherical object waves (a) on-axis and (b) off-axis by using the self-imaging properties of large periodic structures.

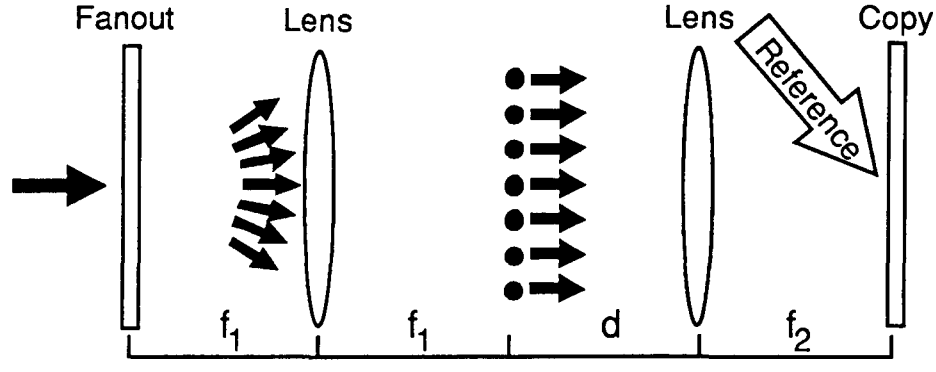

Fig. 9. 4f-system for copying fan-out elements with magnification $m = f_2/f_1$, where $d = f_2$. Focussing power can be included if $d > f_2$.

$\Delta\alpha$	B	$\Delta\varepsilon$	η_T	e	
	1	0.013	0.23	0.63	
0.1°	5	0.017	0.40	0.15	uncorrected
	10	0.018	0.44	0.12	
	1	0.021	0.62	0.20	
0.1°	5	0.022	0.78	0.28	corrected
	10	0.024	0.81	0.30	
0.1°	1	0.021	0.62	0.20	corrected*
	1	0.016	0.32	1.10	
1°	5	0.020	0.55	0.58	uncorrected
	10	0.021	0.60	0.41	
	1	0.024	0.82	0.33	
1°	5	0.026	0.94	0.16	corrected
	10	0.026	0.95	0.12	
1°	1	0.024	0.82	0.32	corrected*
	1	0.024	0.75	1.73	
5°	5	0.026	0.94	0.75	uncorrected
	10	0.026	0.97	0.51	
	1	0.025	0.85	1.35	
5°	5	0.026	0.96	0.80	corrected
	10	0.026	0.97	0.60	
5°	1	0.025	0.96	0.60	corrected*

Table 1. Results for a fan-out of **N = 3.** Maximum useful diffraction efficiency η_T, uniformity error e, and modulation $\Delta\varepsilon$, for different beam ratios B and interbeam angles $\Delta\alpha$. Recording parameters: λ = 0.488 μm, n = 1.5, θ_0 = 30°, d = 15 μm (* see section 5. Discussion).

$\Delta\alpha$	B	$\Delta\varepsilon$	η_T	e	
	1	0.030	0.45	4.20	
0.1°	5	0.050	0.34	4.10	uncorrected
	10	0.038	0.47	3.91	
	1	0.015	0.94	0.19	
0.1°	5	0.015	0.97	0.12	corrected
	10	0.015	0.98	0.12	
0.1°	1	0.015	0.94	0.19	corrected*
	1	0.021	0.30	3.21	
1°	5	0.036	0.41	2.93	uncorrected
	10	0.042	0.42	4.70	
	1	0.015	0.96	1.51	
1°	5	0.015	0.97	0.73	corrected
	10	0.015	0.98	0.57	
1°	1	0.015	0.98	0.35	corrected*
	1	0.024	0.77	1.09	
3°	5	0.016	0.89	0.86	uncorrected
	10	0.016	0.94	0.79	
	1	0.016	0.83	3.95	
3°	5	0.015	0.95	1.68	corrected
	10	0.016	0.97	1.11	
3°	1	0.016	0.83	2.44	corrected*

Table 2. Results for a fan-out of **N = 9.** Maximum useful diffraction efficiency η_T, uniformity error e, and modulation $\Delta\varepsilon$, for different beam ratios B and interbeam angles $\Delta\alpha$. Recording parameters: λ = 0.488 μm, n = 1.5, θ_0 = 30°, d = 15 μm (* see section 5. Discussion).

PROCEEDINGS REPRINT

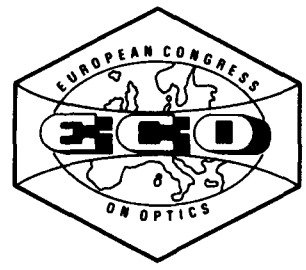

Reprinted from

Optical Interconnections and Networks

14–15 March 1990
The Hague, The Netherlands

ECO3

Volume 1281

HOE for clock distribution in integrated circuits : Experimental results

D. Prongué and H. P. Herzig

University of Neuchâtel, Institute of Microtechnology, CH-2000 Neuchâtel, Switzerland

ABSTRACT

This paper reports the design and fabrication of transmission holographic optical elements (HOEs) for clock distribution. First, we have studied and fabricated a multi-focus doublet HOE. The aberrations due to the wavelength shift between recording ($\lambda = 488$ nm) and reconstruction ($\lambda = 780$ nm) have been minimized by an appropriate recording and readout geometry. The diffraction efficiency has been optimized by a copying technique. Second, we have investigated the near-field internal reflection (TIR) holographic recording technique to solve the problems of miniaturization. With this method, we have recorded a 100×100 lenslet array with focal lengths of $f = 400$ μm.

1. INTRODUCTION

Optical interconnection, using free-space light propagation, allows parallel communication, eliminates mechanical point to point contacts and has the potential of addressing any location on the integrated circuit. Holographic optical elements (HOE) are well suited to realize the required multiple imaging. This paper presents the design and fabrication of transmission HOEs for clock distribution. The basic set-up consists of a signal source (semiconductor laser) and a HOE, which images the source onto photodetectors in the integrated circuit.

The requirements for the HOEs are: low aberrations, low geometrical distortions and high efficiency. In addition, the method to construct the HOEs should be suitable for large numbers of interconnections. Different HOE recording methods will be discussed and some of them are tested experimentally.

Perfect 2-dimensional HOE structures can be generated by computer. To get high efficiencies, however, the computer generated holograms (CGH) have to be transformed into volume or surface-relief HOEs. Problems occur for high spatial frequencies, where Bragg diffraction or blazed structures are difficult to achieve properly. On the other hand, interferometric recording techniques suffer from aberrations caused by the wavelength shift between recording and reconstruction, imposed by the spectral sensitivity of the hologram recording material. Analytical equations, as well as a ray-tracing program have been applied to analyze the geometrical aberrations. The intensity distribution in the image plane has been calculated with the aid of the Rayleigh-Sommerfeld integral. Multiple step recording techniques or CGH wavefront generators can be used to simultaneously compensate the aberrations and fulfill the conditions for high efficiency. However, these techniques are not necessary for small NA and short focal lengths. We have found nearly diffraction limited spot sizes by optimizing the recording geometry of the HOEs.

First, a prototype for clock distribution onto a readily available photodetector array (Fig.2) has been fabricated[1]. The two elements of the doublet HOE are a collimator and a 5×5 multifacet HOE for multiple focussing. This doublet HOE has small aberrations and is insensitive to wavelength variations of the source. The holograms have been recorded at $\lambda = 488$ nm in silver halide emulsions, copied and then

bleached. When reconstructed at $\lambda = 780$ nm, this doublet HOE produces diffraction limited spots of 10 μm diameter. Second, we have investigated the problems of miniaturization. For that purpose, a special test chip was realized at the CSEM (Centre Suisse d'Electronique et de Microtechnique) using CMOS technology and the near-field total internal reflection (TIR) holographic recording technique was introduced. By the same technique a holographic lenslet array with 10'000 interconnection points has been fabricated.

2. HOE DESIGN

The wavelength shift between recording and reconstruction leads to aberrations. As our HOEs are volume holograms, the wavelength shift may also reduce the diffraction efficiency, when the Bragg condition is no longer fulfilled. So, our main goal will be to maintain low aberrations and high diffraction efficiency.

2.1. Analytical equations for the aberrations

The principle parameters (recording and reconstructing angles, astigmatic focal lengths, third order terms) for a HOE can be calculated analytically[1,2]. In this paper, we shall limit ourselves to wavevectors lying in the same plane of incidence, and to plane reference waves ($\rho_r = \rho_R = \infty$), as shown in Fig.1. The direction θ_P of the outgoing wavevector $\mathbf{k}_P$ is given by the grating equation

$$\sin\theta_P = \sin\theta_r \pm m\mu(\sin\theta_O - \sin\theta_R)\,, \qquad (1)$$

where m is the diffraction order (m = +1 in our case), $\mu = \lambda_r/\lambda_R$, and θ_i are the angles of incidence (Fig.1). The indices refer to the waves involved, namely R to the recording reference, O to the object point, r to the reconstructing reference and P to the primary reconstructed wave.

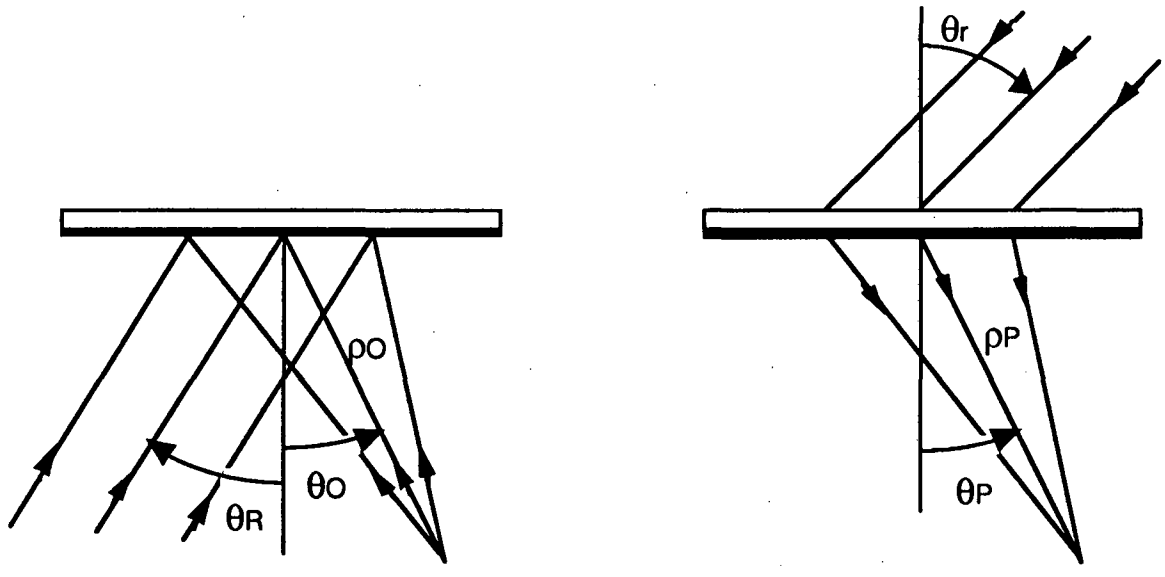

Fig.1 a) HOE recording geometry b) HOE readout geometry.

The principal curvatures of the astigmatic outgoing wave[2] are described by

$$\frac{1}{\rho_P^{\parallel}} = \mu \left(\frac{\cos\theta_O}{\cos\theta_P} \right)^2 \frac{1}{\rho_O}, \qquad \frac{1}{\rho_P^{\perp}} = \mu \frac{1}{\rho_O}, \tag{2}$$

where ρ_i are the radii of curvature measured from the hologram, with $\rho_r = \rho_R = \infty$. The curvature of the astigmatic outgoing wave is given by the principal radii $\rho_P^{\parallel}$ and $\rho_P^{\perp}$, parallel and perpendicular to the plane of incidence, respectively. The outgoing wave is only anastigmatic ($\rho_P^{\parallel} = \rho_P^{\perp}$), if $\theta_O = \theta_P$. Thus, we will keep the angles of the object wave and the image wave equal, in order to eliminate the astigmatic aberration.

With $\rho_P = \rho_P^{\parallel} = \rho_P^{\perp} = \rho_O/\mu$, the third order terms become

$$c_{xxy} = \frac{1}{\cos\theta_P} \left(\frac{1}{\rho_P^2} \sin\theta_P - \frac{\mu}{\rho_O^2} \sin\theta_O \right), \tag{3}$$

$$c_{yyy} = \frac{3}{2\cos^3\theta_P} \times \left(\frac{1}{\rho_P^2} \sin\theta_P \cos^2\theta_P - \frac{\mu}{\rho_O^2} \sin\theta_O \cos^2\theta_O \right), \tag{4}$$

$$c_{xxx} = 0, \qquad c_{xyy} = 0.$$

The coefficients c_{ijk} describe the coma[3]. Note, that the c_{ijk} disappear for a perfect spherical wave. In the off-axis case with conserved geometry ($\theta_P = \theta_O \neq 0°$), there is no astigmatism, but there will be coma. In the on-axis case ($\theta_P = \theta_O = 0°$), coma disappears also.

2.2. Numeric analysis of the aberrations

The analytical equations for wave aberrations allow to determine a suitable geometry, for which the second and third order aberrations are cancelled. But higher order aberrations, more cumbersome to calculate analytically, can still be significant. For this reason, we have used a ray-tracing program. The results are typically presented as spot diagrams (Fig.5). The intensity distribution in the image plane has been calculated with the aid of the Rayleigh-Sommerfeld integral (Fig.6). These computer simulations have shown that cancelling second and third order aberrations was in our case sufficient to get nearly diffraction limited spots, because of the small focal length and aperture.

2.3. Diffraction efficiency

Besides low aberrations of the image wave, the efficiency of the HOE is important. To get high diffraction efficiency, we have to record a volume grating HOE and to fulfill the Bragg condition[6]. The problem is now, that the condition for low aberrations, described above, and maintaining the Bragg condition for a wavelength shift between recording and reconstruction, are not compatible.

Several methods have been proposed in the literature[3,4,5] to satisfy the two conditions more or less simultaneously. They usually involve several steps for the HOE recording, where beams emerge from CGHs or intermediate HOEs. We have opted for a copying technique[1]. In the first step, an intermediate HOE, optimized for low aberrations after the wavelength shift, is recorded. Then, in the second step, this

intermediate HOE is contact copied with another reference beam angle, which allows to adjust the fringe tilt in the new HOE to fulfill the Bragg condition in the center of the facets, while preserving the two-dimensional structure of the fringes.

3. DOUBLET HOE FOR INTERCONNECTION

3.1. Geometrical configuration

For clock distribution, i.e. to focus one source to several locations, a multi-facet HOE is suitable. Each holographic facet contributes to the reconstruction of one single focus point, therefore no intermodulation occurs. Geometrical commodities favor a transmission hologram parallel to the detector plane.

An on-axis geometry ($\theta_O = 0°$) would have the advantage to eliminate third order wave aberrations, while an off-axis geometry (higher spatial frequency) would have higher diffraction efficiency. Both advantages can be brought together by a doublet HOE composed of a collimating HOE and a focusing multi-facet HOE (Fig.2). The two components of the doublet HOE are free of aberrations up to third order, because the divergent source and the convergent image waves are both on-axis, whereas the plane reference waves are off-axis, as desired for high diffraction efficiency.

Pairs of HOEs have been recorded in order to get the following characteristics for the final doublet HOE: readout wavelength $\lambda_r = 780$ nm, collimating focal length $f_1 = 50$ mm, focusing focal length $f_2 = 31$ mm, source wave on-axis ($\theta_{P1} = 0°$), image wave on-axis ($\theta_{P2} = 0°$), plane reference waves at $\theta_r = 30°$, spacing between the HOEs $d = 0$ mm.

3.2. HOE recording

First, a pair of intermediate HOEs (collimating and focusing HOEs) has been recorded at $\lambda_R = 488$ nm on silver halide plates (AGFA 8E56). The geometrical characteristics were: plane reference wave ($\rho_R = \infty$) at $\theta_R = 18.2°$, object wave on-axis ($\theta_O = 0°$) and spherical with $\rho_{O1} = 80$ mm for the collimating and $\rho_{O2} = 50$ mm for the focusing intermediate HOE. The 5×5 facet array of the focusing intermediate HOE has been recorded by step and repeat.

Both intermediate HOE have been contact copied at $\lambda_R = 488$ nm, with a new plane reference wave at $\theta'_R = 24.1°$. At this new reference wave angle the Bragg condition is not satisfied for the intermediate HOE, but the diffraction efficiency is sufficient to record the new HOE.

3.3 Experimental results and simulations

The two HOE were sealed together and illuminated with a laser diode at $\lambda = 780$ nm, as sketched in Fig.2. A picture of the prototype is shown in Fig.3. The reconstructed spots were analyzed using a microscope with a CCD camera mounted on a 3-D translation stage.

Figure 4 shows the center spot and a corner spot generated by the doublet HOE, when illuminated with a laser diode (Hitachi HL7801). The ray-tracing simulation for the same two spots produces the diagrams shown in Fig.5. The diffraction limit, imposed by the aperture of the focusing facets, was calculated approximately as $r \cong \lambda f_2/a = 8.1$ µm, (focal length $f_2 = 31$ mm, facet size $a = 3$ mm, $\lambda = 780$ nm)

and is shown as circles in Fig.5. The intensity distribution in the image plane for the same two spots has been simulated with the aid of the Rayleigh-Sommerfeld integral. The results are shown in Fig.6.

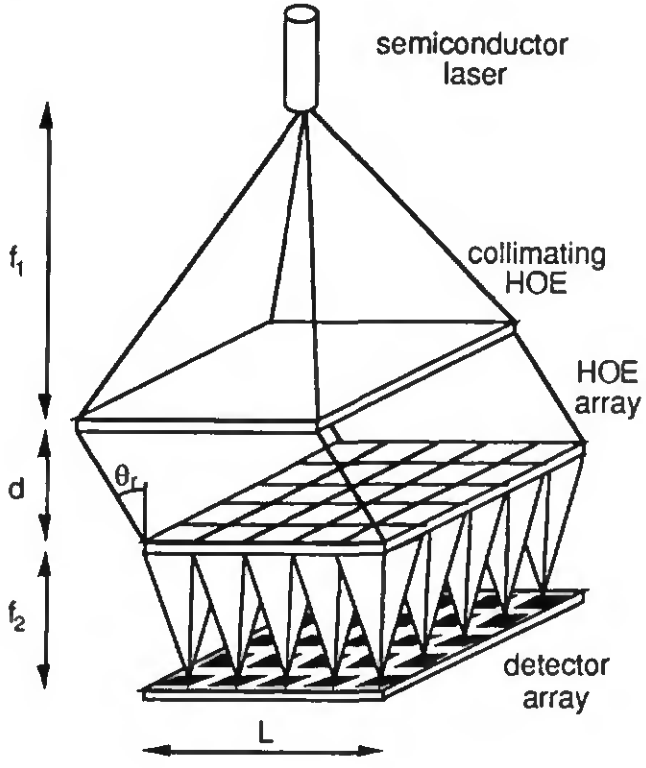

Fig.2 Doublet HOE consisting of a collimation HOE and a focusing HOE array.

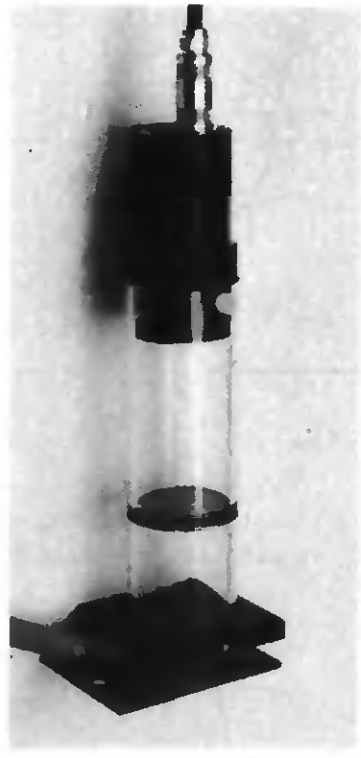

Fig.3 Laboratory prototype corresponding to Fig.2.

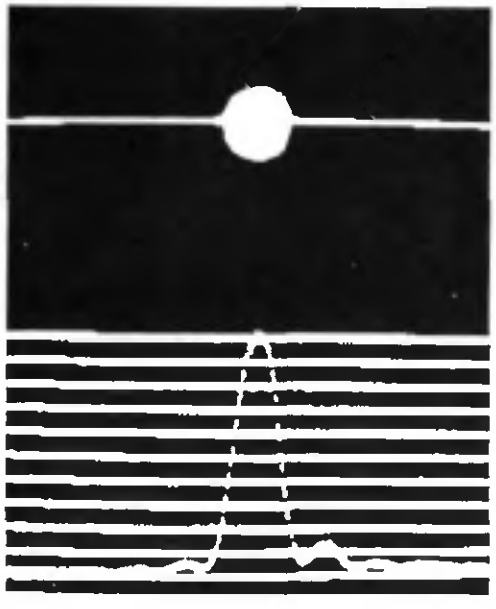

Fig.4 a) Center spot generated by the doublet HOE.

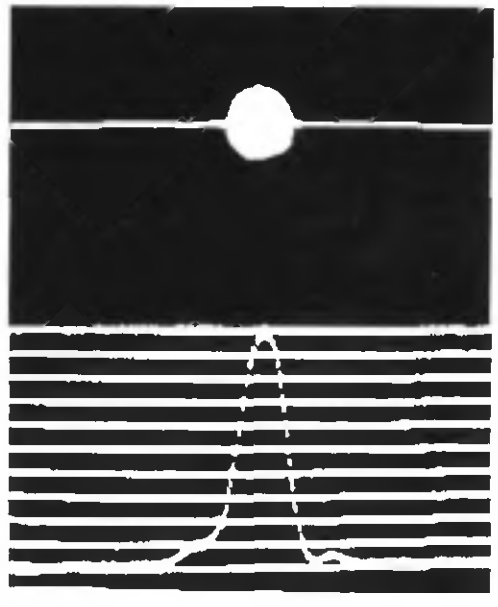

b) Corner spot generated by the doublet HOE.

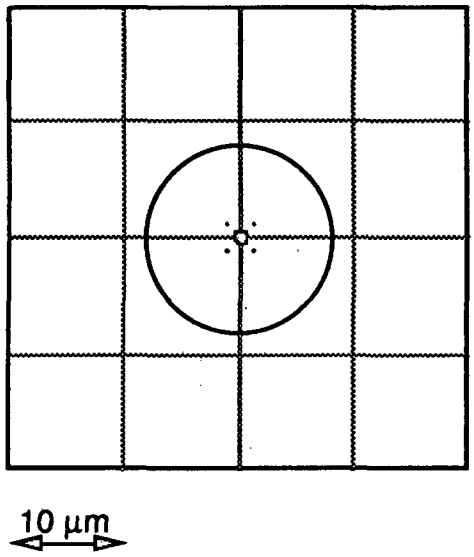

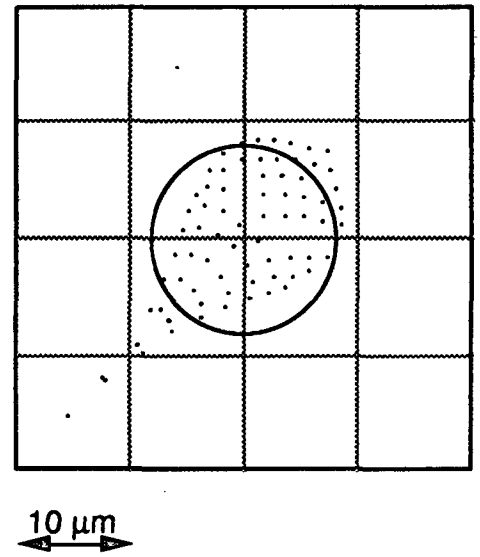

Fig.5 a) Spot diagram of the center spot. The circle indicates the diffraction limit.

b) Spot diagram of the corner spot. The circle indicates the diffraction limit.

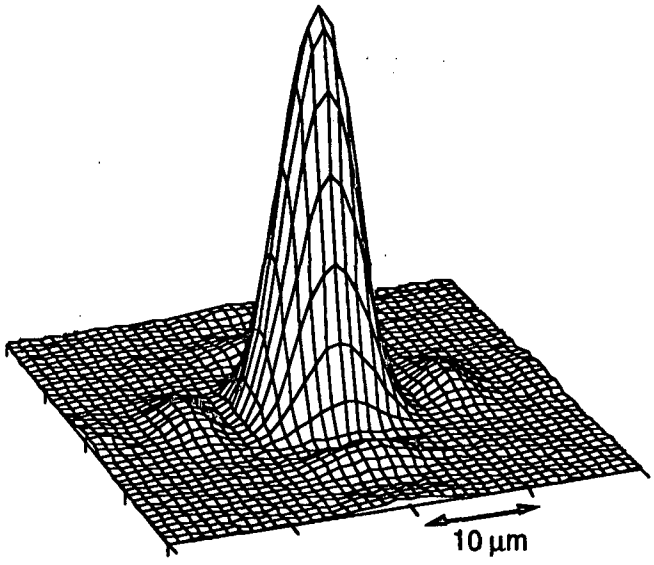

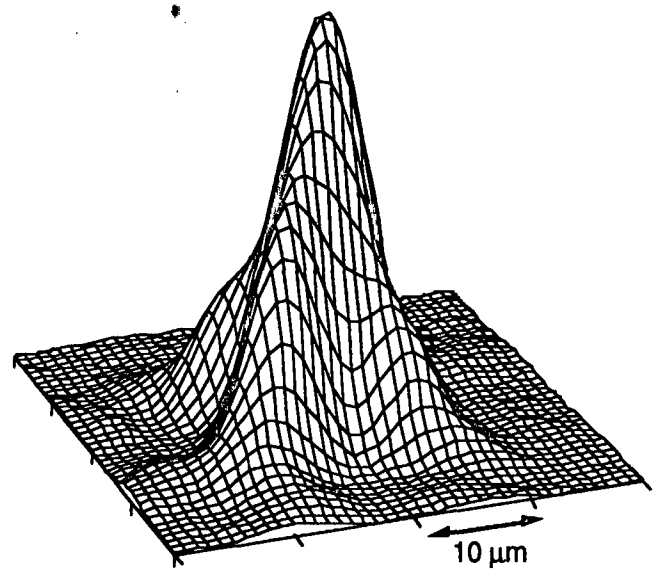

Fig.6 a) Beam profile of the center spot.

b) Beam profile of the corner spot.

4. NEAR FIELD HOLOGRAPHY FOR INTERCONNECTION

The prototype presented in the preceding chapter is of rather large size. Integrated circuits are much smaller. In this chapter we will show how miniaturized lenslet arrays with short focal lengths can be fabricated.

4.1. Principle

Transmission holograms are recorded by interfering an object and a reference wave, where both sources have to be on the same side of the hologram. For recording holographic lenses with short focal lengths, a problem occurs by reasons of geometry. This is overcome by using total internal reflection (TIR) near-field holography, as first reported by Stetson[7]. A mask is recorded holographically by passing a collimated beam through the mask, which is placed in close proximity (typically 50 - 500 μm) to the photosensitive layer (Fig.7). The transmitted wave interferes with the reference wave, which is fed through a prism and totally reflected at the film-air interface. An array of pinholes is fabricated as a chrome on glass mask by electron beam lithography. When illuminated with a plane wave, the mask generates by diffraction an array of spherical waves. This technique assures a position accuracy of about 0.2 μm between the light spots. For the reconstruction without prism, the readout beam can be coupled into the hologram substrate by a small prism or another holographic grating, which acts also as collimator. This coupling element can be fabricated in the same film as the lenslet array. Collimator and lenslet array form together a compact system, as shown in Fig.8. Because of its symmetry, this system is quite insensitive to wavelength changes.

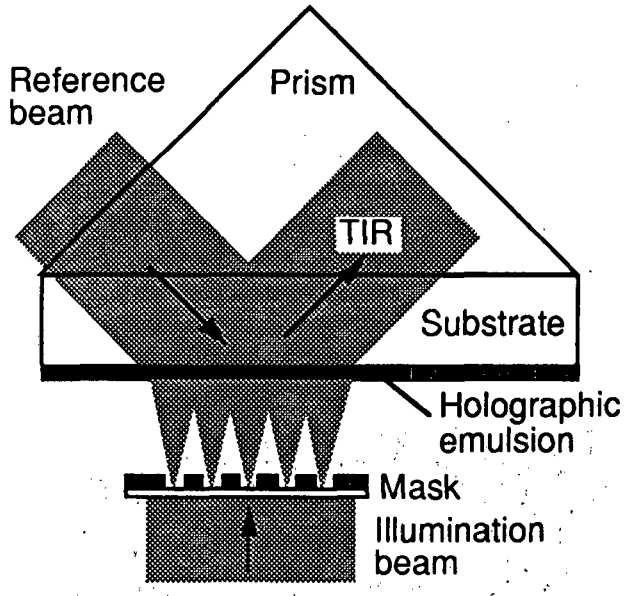

Fig.7 Near-field TIR recording geometry.

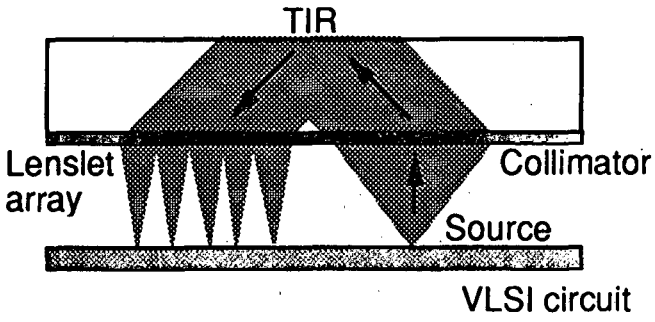

Fig.8 Compact system for near-field TIR doublet HOE.

4.2. Lenslet array

To test the performance of the TIR method, we have fabricated a 100 x 100 array of lenslets, equally distributed on a surface of 1 cm^2, which corresponds to a spacing of 100 μm between the spots. Each holographic lens has a focal length of f = 390 μm, and a diffraction limited spot size of Ø = 10 μm. Figure 9 shows a part of the generated spot pattern.

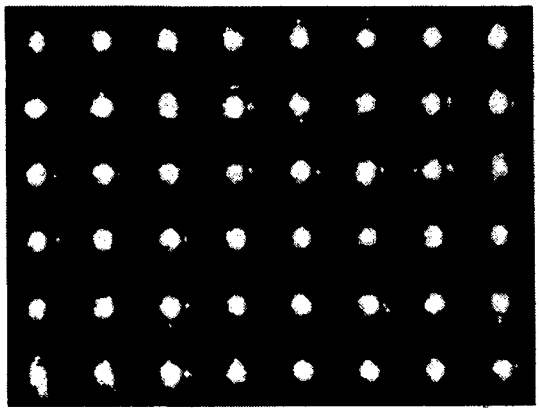

Fig.9 Partial image of the 100×100 lenslet array.

4.3 Interconnection results

Actually we apply the TIR method to fabricate a non-regular lenslet array for demonstrating clock distribution in an integrated circuit. We will give here some preliminary results.

For that purpose, a special test chip, shown in Fig.10, has been realized at the CSEM (Centre Suisse d'Electronique et de Microtechnique) using CMOS technology (CMN20A of VTI). Its outer dimensions are 3 mm × 3 mm. Several arrays of photodetectors with different sizes from 100 μm × 100 μm down to 3 μm × 3 μm are integrated on the chip. The chip contains also transimpedance amplifiers and output buffers to interface the photodiodes to the external analyzing system.

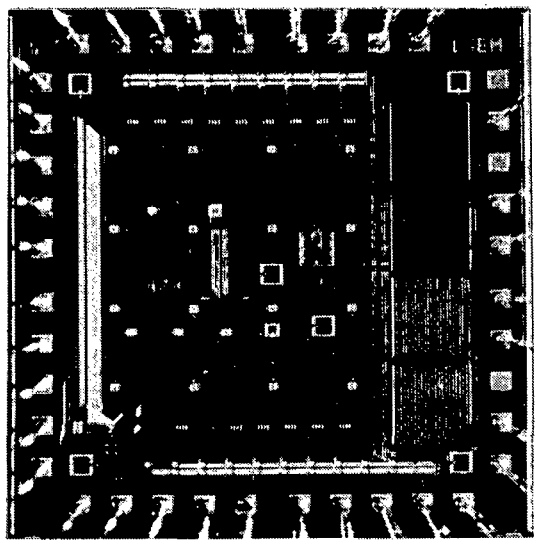

Fig.10 VLSI chip realized by the CSEM.

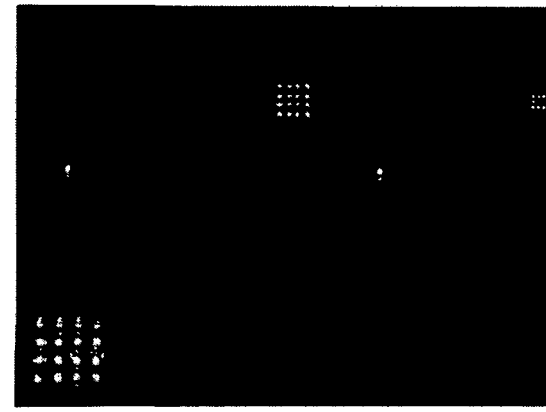

Fig.11 Partial image of the corresponding lenslet array.

The chrome mask to record the HOE has been fabricated by e-beam lithography. The detectors are now replaced by holes, where each hole acts as source when illuminated with a laser beam. The HOE has been

recorded in a DuPont photopolymer. Figure 11 shows the reconstructed spot pattern at $\lambda = 488$ nm. One can see that all patterns are reconstructed properly. It has been demonstrated recently[8], that the TIR method is capable to reproduce structures down to 0.4 μm for $\lambda = 488$ nm.

4.4 TIR method for the IR

The TIR method requires a recording angle of typically 45°, which is larger than the angle for total reflection in glass. For large wavelength shifts between recording and reconstruction, the readout angle may then become larger than 90°. This is the case if the hologram is recorded at $\lambda = 488$ nm (dichromated gelatine, photopolymer) and reconstructed at $\lambda = 780$ nm (GaAlAs-laser). However, in that case the hologram can be recorded first at $\lambda = 633$ nm in a silver halide emulsion and then copied without the prism at 488 nm in dichromated gelatine (DCG) or photopolymer. In the copying process the Bragg angle can be readjusted, as reported in a previous paper[1].

5. DISCUSSION

It has been shown with the doublet HOE configuration, that phase aberrations up to third order can be cancelled. Second order aberrations are eliminated by choosing the same angle for the image (θ_P) and the object (θ_O), third orders by choosing an on-axis set-up ($\theta_P = \theta_O = 0°$). But, it is not possible to cancel all aberrations for the entire HOE if only plane and spherical wave fronts are used to record and replay the HOE. However, we could minimize the aberrations (all orders together) by optimizing the recording geometry, using a ray-tracing program and the root mean square radius as criteria.

The Bragg condition and the condition for low aberrations are only fulfilled rigorously near the center of the HOE. Since in our case the aperture of the focusing facets are small, the spots are nearly diffraction limited and the Bragg mismatch at the borders of the HOE is small enough to give nearly optimum diffraction efficiency. Note that, for the same numerical aperture (NA), the aberrations decrease with smaller system size, i.e. with shorter focal length.

For higher numerical apertures, the aberrations will certainly prevail over the diffraction limit and determine the spot sizes. Then, it will be very important to minimize all aberrations. The Bragg mismatch will become significant at the borders of the HOE and the HOE diffraction efficiency will decrease. In this case, aspherical wave fronts for recording the HOE must be used to minimize the aberrations and to fulfill the Bragg condition simultaneously. These wave fronts can be provided by computer generated holograms (CGH)[5].

The automatic step and repeat system for the recording of holographic lenslet arrays can provide a nearly unlimited number of focal spots. In addition, the generated pattern needs not to be regular. The light intensity of each spot can be controlled by the aperture during recording, which determines also the spot size. The TIR holography is very powerful to record very large numbers of regularly spaced facets with very short focal lengths. The numerical aperture of the pinholes and the distance between mask and HOE have to be appropriately chosen to avoid large overlapping of the diffraction patterns, which would cause intermodulations.

Compared with computer generated lenslet arrays[9], the holographic method (recording by interference) has the advantage that holographic materials with very high resolution can be used. Recording gratings with more than 2000 lines/mm is standard for materials such as DCG, photopolymers and photoresist.

6. CONCLUSION

A prototype of a 5×5 holographic lens array operating at $\lambda = 780$ nm has been fabricated with a doublet HOE. The doublet HOE is free of aberrations up to third order and works under Bragg condition. It would perfectly feed a 5×5 array of 10×10 μm^2 large detectors. The recording geometry is simple and a step and repeat process is used for the array.

We have investigated the near-field total internal reflection (TIR) holographic recording technique to solve the problems of miniaturization. With this method a holographic lenslet array of 10'000 interconnection points with short focal lengths of $f = 390$ µm and spot sizes of 10 µm has been fabricated successfully.

Finally, the TIR method has been applied to the clock distribution on a specially designed VLSI circuit.

7. REFERENCES

1. D. Prongué, H. P. Herzig, "Design and fabrication of HOE for clock distribution in integrated circuits," *Proc. of the International Conference on Holographic Systems*, IEE Publication No. 311, pp. 204-208, 1989.

2. H. P. Herzig, R. Dändliker, "Holographic optical scanning elements: analytical method for determining the phase function", *J. Opt. soc. Am. A*, 4, pp. 1063-1069, 1987.

3. H. P. Herzig, "Holographic optical elements (HOE) for semiconductor lasers", *Opt. commun.*, 58, pp. 144-148, 1986.

4. M. Assenheimer, Y. Amitai and A. A. Friesem, "Recursive design for an efficient HOE with different recording and readout wavelength", *Appl. Opt.*, 27, pp. 4747-4752, 1988.

5. H. Buczek, J. M. Teijido, "Application of electron-beam lithography at CSEM for fabricating computer-generated holograms", *SPIE 884*, pp. 46-51, 1988.

6. H. Kogelnik, "Coupled wave theory for thick hologram gratings", *Bell. Syst. Tech. J.*, 48, pp. 2909-2947, 1969.

7. K. Stetson, "Holography with total internally reflected light", *Appl. Phys. Lett.*, 11, pp. 225-226, 1967.

8. R. Dändliker, J. Brook, "Holographic photolithography for submicron VLSI structures", *Proc. of the International Conference on Holographic Systems*, IEE Publication No. 311, pp. 127-132, 1989.

9. M. R. Feldman, C. C. Guest, "Computer generated holographic optical elements for optical interconnection of very large scale integrated circuits", *Appl. Opt.*, 26, pp. 4377-4384, 1987.

Optimized kinoform structures for highly efficient fan-out elements

D. Prongué, H. P. Herzig, and R. Dändliker
Institute of Microtechnology, University of Neuchâtel, CH-2000 Neuchâtel, Switzerland
M. T. Gale
Paul Scherrer Institute, Badenerstrasse 569, CH-8048 Zürich, Switzerland

Abstract

This paper deals with the realization of highly efficient fan-out elements. Laser-beam writing lithography is now available for fabricating smooth surface relief microstructures. We have developed several methods to optimize the microstructure profiles. Only a small number of parameters in the object plane are necessary to determine the kinoform. This simplifies the calculation of M×N arrays also for large M and N. Experimental results for a 9 beam fan-out element are presented.

Key words: fan-out, kinoform, phase grating, CGH, HOE.

Accepted for publication in Applied Optics, Vol. 31, 1992

I. Introduction

Phase elements generating arrays of light spots are key components in many optical processing systems. Space invariant fan-out elements split a laser beam into N quasi plane waves, which are focused by a Fourier lens as shown in Fig. 1.

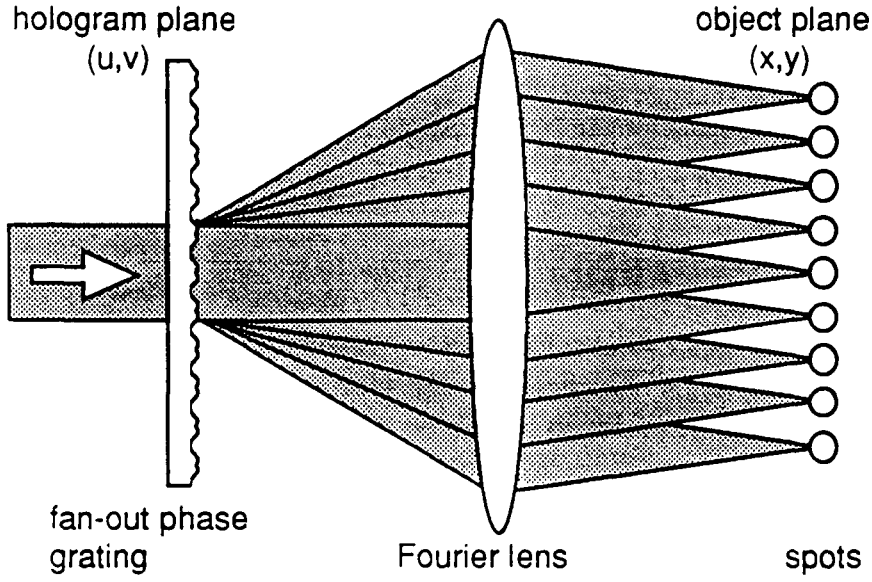

Fig. 1. Readout of the fan-out element.

Different types of fan-out elements have been investigated in the past. Binary phase holograms, such as Dammann gratings, are well known. Their fabrication involves microlithographic techniques which are well mastered and widely available. However, these elements are usually limited by their efficiency. To increase the diffraction efficiency, recent efforts have concentrated on multilevel phase structures, such as quaternary phase elements[1] or off-axis multilevel phase elements[2]. Their fabrication also involves microlithography, but with the drawback that the number of masks increases with the number of phase levels. Thus, very precise alignment has to be performed at each process.

In our approach, we optimize a non-quantized phase transfer function for an on-axis fan-out element and we implement this phase function as a smooth surface relief grating. This process became possible with the laser-beam writing system developed at the Paul Scherrer Institute Zürich (PSIZ)[3,4]. This method has the advantage that smooth surfaces can be generated, which can have maximum diffraction efficiency, and that the structure is drawn in one single step, which avoids errors due to successive alignments. On the other hand, the control of the modulation depth can be difficult, depending on the knowledge and stability of the photoresist and development parameters.

We have developed a two step method to optimize the transfer function of a fan-out element[5,6]. The optimization criteria are the efficiency and the uniformity of the outgoing beams. The parameters to optimize are the amplitudes and phases of an array of recorded virtual light sources. These sources are called virtual, because they are only used to describe the construction of the fan-out element, but they are not physically used to record the fan-out element. The small number of free parameters and the non-quantized phase function in the hologram plane leads to very fast optimization procedures.

We applied the optimization method to a 9 beam fan-out and we recorded its transfer function into photoresist. The resulting element is an on-axis surface relief phase hologram.

II. Kinoform optimization

The goal of our fan-out element is to focus a laser beam into a regular array of equally intense light spots. The desired field distribution in the object plane (Fig. 1) is then given by

$$U(x,y) = \sum_{m=1}^{N} A_m \exp[i\phi_m]\, \delta(x - x_m, y), \tag{1}$$

where A_m is the amplitude, ϕ_m the phase, and x_m the position of the m-th spot of a 1D array. The phases ϕ_m are free parameters.

The field distribution $\hat{U}(u,v)$ in the hologram plane is related to the field $U(x,y)$ by a Fourier transform:

$$\begin{aligned}\hat{U}(u,v) &= \int_{-\infty}^{\infty} U(x,y) \exp[2\pi i(xu + yv)]\, dxdy \\ &= \sum_{m=1}^{N} A_m \exp[i\phi_m] \exp[2\pi i x_m u].\end{aligned} \tag{2}$$

The field $\hat{U}(u,v)$ written in terms of magnitude and phase is

$$\hat{U}(u,v) = |\hat{U}(u,v)| \exp[i\psi(u,v)], \tag{3}$$

where $\psi(u,v) = \arg\{\hat{U}\}$. For the irradiance distribution $I(u,v)$ in the hologram plane we obtain

$$I(u,v) = |\hat{U}(u,v)|^2 = \sum_{m=1}^{N} A_m^2 + 2\sum_{m<n}^{N} A_m A_n \cos(\Omega_{mn}), \tag{4}$$

where the arguments Ω_{mn} stand for

$$\Omega_{mn} = 2\pi u(x_m - x_n) + \phi_m - \phi_n. \tag{5}$$

For a constant distance s between the spots the arguments Ω_{mn} in Eq. (5) become

$$\Omega_{mn} = 2\pi u(m-n)s + \phi_m - \phi_n. \tag{6}$$

The first term on the right side of Eq. (4) is constant and equal to the mean object irradiance

$$\langle I \rangle = \langle |\hat{U}|^2 \rangle = \sum_{m=1}^{N} A_m^2. \tag{7}$$

The second term describes the irradiance variations, or intermodulations, in the hologram plane.

To perfectly reproduce the desired object $U(x,y)$, the hologram must have a transfer function proportional to $\hat{U}(u,v)$, which means an intensity transfer function proportional to $I(u,v)$ and a phase transfer function equal to $\exp[i\psi(u,v)]$. With a single hologram, the intensity transfer function can only be made by absorption. This will inevitably reduce the efficiency.

The losses due to absorption by the intensity transfer function are minimized if the variations of the object irradiance in the hologram plane are minimized, i.e.

$$\iint [I(u,v) - \langle I \rangle]^2 \, dudv \rightarrow \min. \tag{8}$$

Because we are only interested in the intensity distribution of the object, the phases ϕ_m are free parameters. To determine the optimum phases, the irradiance I(u,v) given by Eq. (4) is introduced into Eq. (8). We get

$$\iint \left(\sum_{m<n}^{N} A_m A_n \cos(\Omega_{mn}) \right)^2 dudv \rightarrow \min., \tag{9}$$

which means that the intermodulation terms have to be minimized. The intermodulation terms can be rewritten by collecting terms of the same spatial frequency, namely

$$\begin{aligned} \sum_{m<n}^{N} A_m A_n \cos(\Omega_{mn}) &= \sum_{k=1}^{N-1} \sum_{m=1}^{N-k} A_m A_{m+k} \cos(2\pi k s u + \phi_m - \phi_{m+k}) \\ &= \sum_{k=1}^{N-1} B_k \cos(2\pi k s u + \Phi_k), \end{aligned} \tag{10}$$

where $k = m - n$. The coefficients B_k are obtained from

$$\begin{aligned} B_k^2 = &\left(\sum_{m=1}^{N-k} A_m A_{m+k} \cos(\phi_m - \phi_{m+k}) \right)^2 + \\ &\left(\sum_{m=1}^{N-k} A_m A_{m+k} \sin(\phi_m - \phi_{m+k}) \right)^2. \end{aligned} \tag{11}$$

Equation (9) becomes then

$$\iint \left(\sum_{k=1}^{N-1} B_k \cos(2\pi k s u + \Phi_k) \right)^2 dudv \rightarrow \min. \tag{12}$$

Since the intermodulations terms $B_k \cos(2\pi k s u + \Phi_k)$ in Eq. (12) have different spatial frequencies, they are orthogonal and therefore one gets from Eq. (12)

$$\sum_{k=1}^{N-1} B_k^2 \rightarrow \min. \tag{13}$$

Equation (13) supplies together with Eq. (11) the criterion to determine the optimum phases ϕ_m for the fan-out element with maximum efficiency.

The criterion in Eq. (13) reduces the intermodulation terms of Eq. (4) to a minimum, but there is still a residual intermodulation. However, to avoid any absorption in the hologram plane, and also for fabrication reasons, we opt for a pure phase element. The phase is implemented as a smooth surface relief hologram without quantization. Thus, the intensity transfer function of the fan-out element is clipped to I(u,v) = 1. The phase transfer function is equal to $\exp[i\psi(u,v)]$, as obtained for the optimum phases ϕ_m from Eqs. (2) and (3).

Clipping the residual intermodulation terms does hardly alter the high efficiency, but reduces the uniformity of the fan-out. The amplitudes A'_m of the reconstructed spots are slightly different from the desired amplitudes A_m assumed for the recorded virtual light sources (Fig. 2). Furthermore, some weak side spots appear on each side of the desired N beams.

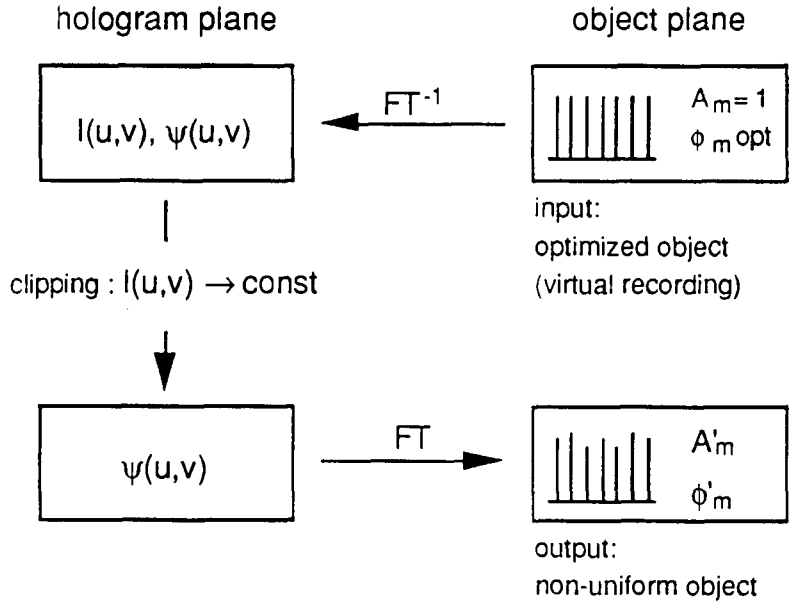

Fig. 2. First optimization process for the phases ϕ_m to get high efficiency. The reconstructed object after clipping is non-uniform ($A'_m \neq 1$).

There are different solutions to solve the uniformity problem. One is to add additional weak light spots to the virtual recording light sources. Thus, the new parameter set contains N' ($N' > N$) light sources, where the intensity of only N object beams are of interest. Now, the minimum of Eq. (8) can be significantly reduced. The effect of clipping becomes negligible. The readout of this fan-out produces N' light spots with perfect uniformity of the amplitudes A_m for $m = 1$ to N. On the other hand, the N'–N additional light spots (A_i, ϕ_i) increase the number of optimization parameters. As a result, the computing time rises strongly. Therefore, to improve the uniformity of the fan-out, we propose another optimization process. By changing the amplitudes of the recorded virtual light sources slightly to $A_m^{(n)}$, the resulting amplitudes $A'^{(n)}_m$ in the output can be balanced; the efficiency decreases not much.

In the following we demonstrate the optimization step by step.

III. Application of the optimization

First optimization

For weighted fan-outs, any distribution of the A_m can be assumed and optimized following the procedure described above. However, we treat here only the particular case of uniform fan-outs ($A_m = 1$). For symmetry considerations, we impose an even distribution of the phases ($\phi_m = \phi_{N+1-m}$). In this case, Eq. (11) reduces to :

$$B_k = \sum_{m=1}^{N-k} \cos(\phi_m - \phi_{m+k}). \qquad (14)$$

From Eqs. (13) and (14) we get the optimum phases ϕ_m. The minimum in Eq. (13) is found by numerical optimization, using the Downhill Simplex Method[7]. Figure 3 shows the optimization procedure and Table 1a) lists the optimum phases ϕ_m.

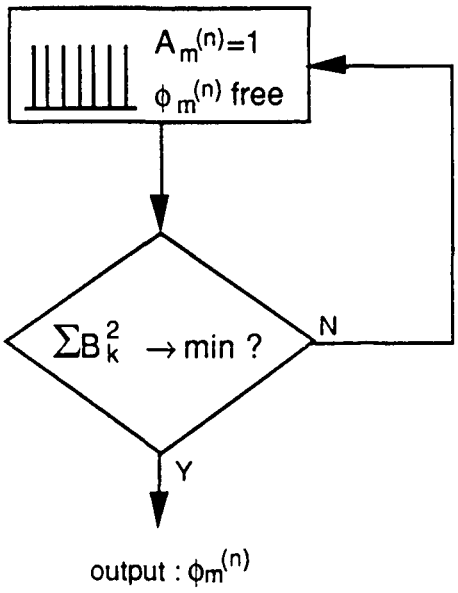

Fig. 3. Numerical optimization of phases for maximum efficiency.

From the optimized set of phases ϕ_m, the field $\hat{U}(u,v)$ in the hologram plane and the corresponding intensity I(u,v) and phase $\psi(u,v)$ are obtained through Eqs. (2) and (3). After clipping the intensity transfer function to $I(u,v) = 1$, we get a phase only fan-out element with phase $\psi(u,v)$ shown in Fig. 4. We calculate the reproduced field in the object plane, which consists now of N spots with amplitudes $A'_m \neq 1$, as listed in Table 1b). The uniformity error is due to the clipping of the residual intermodulation terms in the intensity transfer function I(u,v) of the hologram (Fig. 2).

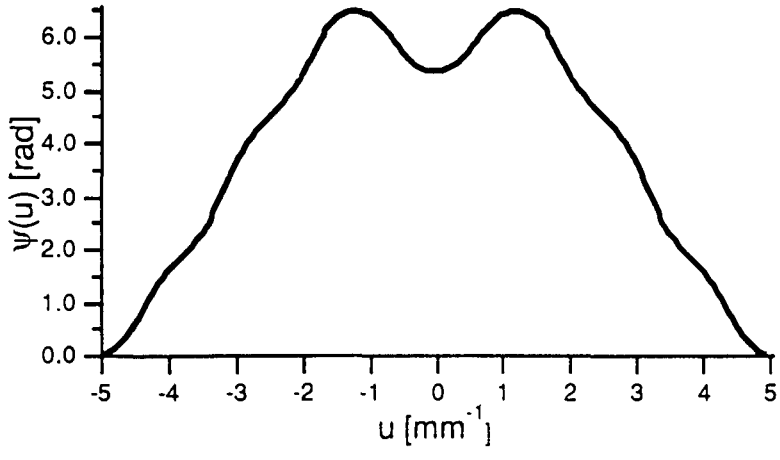

Fig. 4. Phase transfer function $\psi(u,v)$ of a high efficiency 9 beam fan-out element.

For a 9 spot fan-out element, this first optimization leads to 99.38% of the incident light diffracted into the 9 beams with ±5.35% uniformity error.

We have imposed above, a symmetrical distribution of phases ($\phi_m = \phi_{m+1}$). Optimization runs without this restriction have also been performed. For odd fan-out numbers, we did never find higher efficiencies with non-symmetrical phases. However for even fan-out numbers, we did

find higher efficiencies with non-symmetrical phases. Therefore the restriction of symmetrical phase has been dropped for the even fan-out numbers.

If the uniformity is more important than the efficiency, we continue with the second optimization step.

	a) optimum virtual recording spots		b) outgoing spots	
m	A_m	ϕ_m	A'_m	ϕ'_m
1	1	1.772	0.947	1.772
2	1	0.135	0.994	0.136
3	1	3.887	0.991	3.887
4	1	2.455	1.000	2.453
5	1	3.142	0.964	3.142
6	1	2.455	1.000	2.453
7	1	3.887	0.991	3.887
8	1	0.135	0.994	0.136
9	1	1.772	0.947	1.772

Table 1. Highly efficient 9 beam fan-out element:
a) amplitude and phase of the virtual recording light sources,
b) amplitude and phase of the resulting light spots.

Second optimization

The uniformity errors can be minimized by a second optimization procedure shown in Fig. 5. We will now maintain the optimum phases ϕ_m from the first optimization and change the amplitudes A_m, until perfect uniformity in the reproduced image ($A'_m = 1$) is obtained, after clipping I(u,v) in the hologram plane. The amplitudes $A_m^{(n)}$ of the virtual sources are changed individually at each iteration loop of the optimization process to correct for the non-uniform amplitudes $A'_m{}^{(n)}$ of the diffracted spots. The virtual source amplitudes $A_m^{(n+1)}$ for the next iteration are obtained from

$$A_m^{(n+1)} = A_m^{(n)} \frac{\langle A'_m{}^{(n)} \rangle}{A'_m{}^{(n)}}, \qquad (15)$$

where $\langle A'_m{}^{(n)} \rangle$ is the average over all diffracted amplitudes. The ratio $A'_m{}^{(n)}/\langle A'_m{}^{(n)} \rangle$ represents the weight of the m^{th} diffracted amplitude and serves as the correction factor for the next iteration (n+1). The new optimized set of the amplitudes A_m and phases ϕ_m, of the virtual sources for the 9 beam fan-out element is shown in Table 2a).

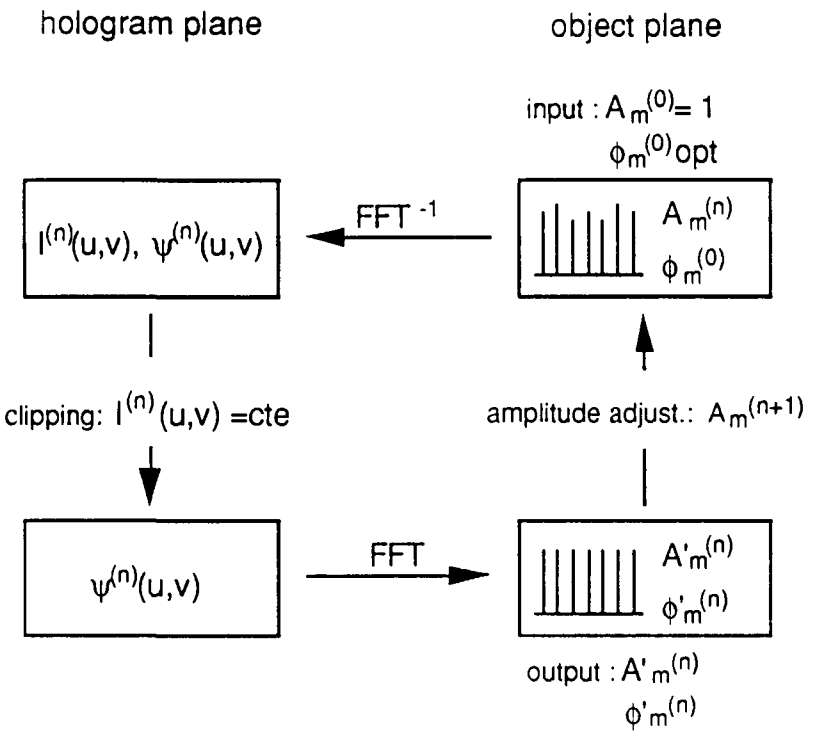

Fig. 5. Second optimization step (uniformity):
$\phi_m^{(0)}$ comes from the first optimization step,
(n) counts the number of iterations.

This parameter set produces the intensity I(u,v) and the phase $\psi(u,v)$ in the hologram plane. After clipping (I(u,v) = I), the reproduced spot amplitudes are perfectly uniform (see Table 2b). The fan-out phase distribution $\psi(u,v)^{(n)}$ is very similar to the one shown in Fig. 4. This second optimization has reduced the efficiency only slightly from 99.38% to 99.28%.

	a) optimum virtual recording spots		b) outgoing spots	
m	$A_m^{(n)}$	$\phi_m^{(n)}$	$A'^{(n)}_m$	$\phi'^{(n)}_m$
1	1.059	1.772	1.000	1.769
2	0.957	0.135	1.000	0.134
3	0.987	3.887	1.000	3.888
4	0.998	2.455	1.000	2.451
5	1.022	3.142	1.000	3.155
6	0.998	2.455	1.000	2.451
7	0.987	3.887	1.000	3.888
8	0.957	0.135	1.000	0.134
9	1.059	1.772	1.000	1.779

Table 2. Perfectly uniform 9 beam fan-out element:
a) amplitude and phase of the virtual recording light sources,
b) amplitude and phase of the resulting light spots.

IV. Discussion

Results of numerical optimization

We have applied our optimization methods to fan-out elements with different numbers N of beams. The computed efficiencies and uniformities resulting from the first and second optimization are shown in Table 3.

	efficiency optimization		uniformity optimization	
N	η [%]	ΔI_m [%]	η [%]	ΔI_m [%]
3	94.9	±23.0	92.6	<0.1
5	98.0	±28.2	92.1	<0.1
7	98.0	±22.3	96.8	<0.1
9	99.4	±5.4	99.3	<0.1
10	98.2	±30.6	95.4	<0.1
11	98.8	±21.6	97.7	<0.1
13	99.3	±27.3	96.3	<0.1
21	99.2	±16.9	98.6	<0.1
81	99.3	±20.7	97.0	<0.1
100	98.8	±32.7	97.4	<0.1
101	99.1	±26.8	98.0	<0.1
117	99.2	±43.4	97.6	<0.1

Table 3. Efficiency and uniformity issued from first and second optimization.

For the 9 beam element, the computing time on a MicroVAX 3400 was about 250 ms for the efficiency optimization and about 900 ms for the uniformity optimization. The computing time for large fan-outs can be considerably reduced by choosing a good starting parameter set. Good starting sets can be obtained by cascading optimum solutions of smaller fan-outs, as shown in Fig. 6. For example, an efficient 117 beam fan-out is obtained by cascading the two optimized solutions for N = 9 and N = 13.

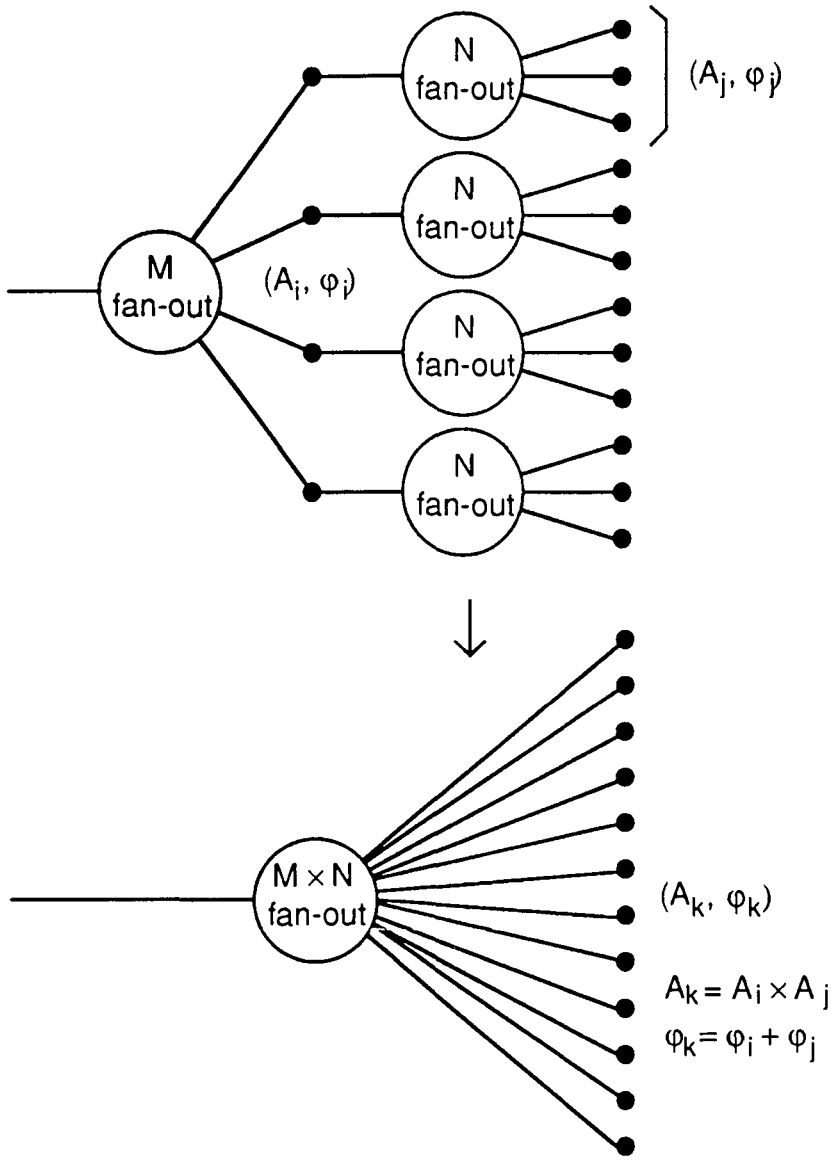

Fig. 6. Cascading parameter sets.

Adding or subtracting a few points in the solution for a large optimized fan-out gives also a good starting parameter set. For example, the 100 beam fan-out has been obtained just by taking away one virtual source in the optimum solution for 101 beams.

Although the results of the optimization have only been implemented for a one-dimensional on-axis element, they can also be used for two-dimensional elements and for off-axis elements. The two-dimensional $M \times N$ parameter set is defined by $A_{ij} = A_i A_j$ and $\phi_{ij} = \phi_i + \phi_j$, where $i \in [1..M]$ and $j \in [1..N]$. For example, an optimized 9×9 fan-out element leads to 98.6% efficiency with perfect uniformity.

Reflection fan-out elements can be obtained by deposition of a reflective coating on a specially designed kinoform relief. Another solution is to replay the fan-out element under total internal reflection (TIR) conditions. Such elements do not need special reflective coatings and are of great interest for integrated planar optics. 2D and TIR fan-out elements are actually under investigation.

Another interesting type of elements combines fan-out and focusing properties. Focusing can be added by a Fresnel lens superposed to the fan-out phase structure, the whole structure being written in one raster scan.

The photoresist relief structure of all elements discussed above, can be converted into a metal master relief by electroplating techniques for mass-production of low-cost replicas.

V. Comparison with other optimization procedures

The first and second optimization steps described in this paper are fast. They lead to fan-out elements with good efficiency and perfect uniformity. Some other optimization procedures have also been tested for comparison.

Amplitude optimization

In the described first optimization step we minimize the variance of the object irradiance in the hologram plane (Eq. 8). Wyrowski defines an upper limit for the diffraction efficiency of phase only holograms (Eq. (19b) of Ref. 8). This upper limit is reached when the variations of the object field amplitude $|\hat{U}|$, around its average value $\langle|\hat{U}|\rangle$, are minimum. This leads to a different optimization criterion, namely

$$\int\int (|\hat{U}| - \langle|\hat{U}|\rangle)^2 \, du dv \rightarrow \min. \qquad (16)$$

We have optimized a few fan-outs following this criterion. The optimization process was much slower. It yields the same set of optimum phases.

Phase spectrum optimization

In this optimization, we work with a set of parameters defined in the hologram plane. The grating phase function is constructed from a limited sum of harmonics:

$$\hat{U}(u,v) = \exp[i\psi(u,v)], \qquad (17)$$

$$\psi(u,v) = \sum_{p=1}^{P} A_p \cos[2\pi p u]. \qquad (18)$$

The amplitudes A_p of these harmonics are the optimization parameters, while the efficiency and the uniformity in the object plane are the criteria for the optimization. Again, this optimization process is much slower. For a 5 beam fan-out element, built with the 10 first odd harmonics, 3 minutes of computing time on a MicroVAX 3400 was necessary to find the same optimum phase function with 92.1% efficiency and <0.1% uniformity error as already shown in Table 3. However, this method is more general and can easily take into account the limitations for the resolution of the hologram writing system by limiting the number of harmonics.

VI. Kinoform fabrication

The above results can be used for the fabrication of either on-axis or off-axis holograms (recorded with a reference beam). For our application we have opted for an on-axis hologram where the phase function is transferred into photoresist as a surface relief element. By the time of fabrication of the kinoform, only the first optimization step had been developed. Therefore only the phase $\psi(u,v)$ resulting from the first optimization has been implemented.

The element was fabricated at the Paul Scherrer Institute Zürich (PSIZ), where a high precision laser-beam writing system is available[4]. A photoresist layer is deposited on a flat substrate. It is exposed with a scanning laser beam of controllable intensity. Then it is etched in developer.

The etching rate depends on the received exposure dose. The fidelity of the relief phase element relies on the knowledge and reproducibility of the photoresist response. Finally the phase element is baked and measured with a stylus profilometer. One typical measured profile of photoresist thickness is shown in Fig. 7.

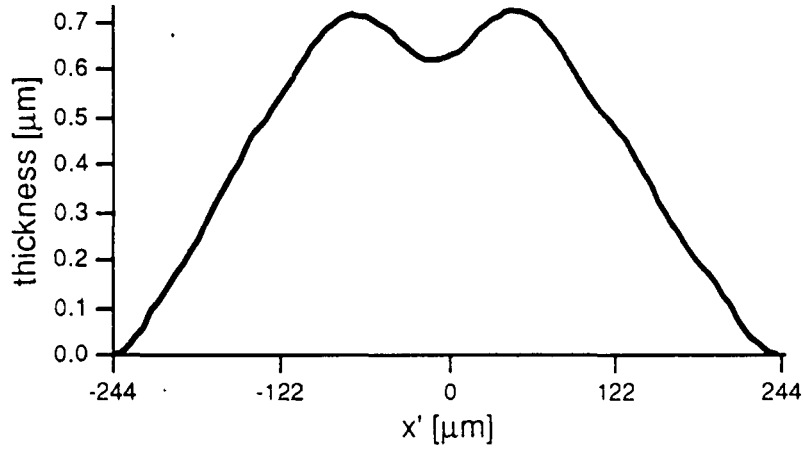

Fig. 7. Profile thickness of the fabricated fan-out.

The element has been tested by analyzing the Fourier image produced when illuminated with a plane wave laser beam (Fig. 1). The diffracted beams are focused onto a CCD camera with a lens of 100 mm focal length. The measured relative values of the spot intensities are shown in Fig. 8. The uniformity is within ±7%. The absorption of the substrate and the photoresist has been measured to be 2%. The measured efficiency, i.e. the fraction of the transmitted light focused into the 9 spots, was 92%.

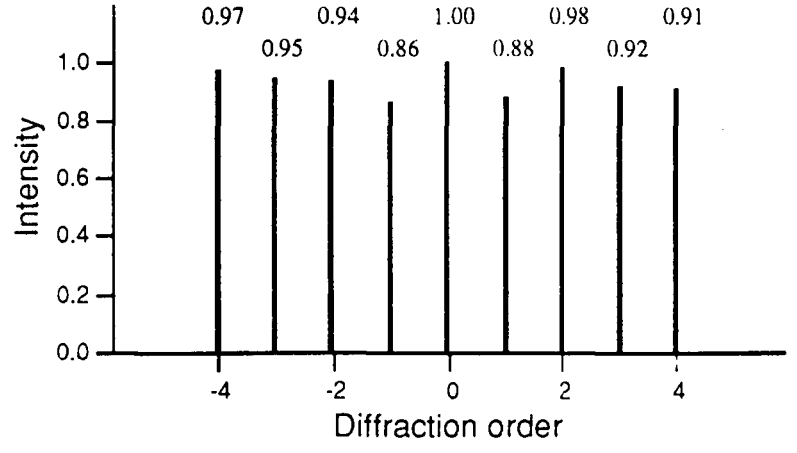

Fig. 8. Relative intensities of the fabricated fan-out.

VII. Conclusions

A two step method to optimize the transfer function of fan-out elements has been developed. The first step optimizes the efficiency. The result is an element with minimized variations of the intensity transfer function. To get a pure phase element, the residual intermodulations in the intensity transfer function are clipped. This introduces uniformity errors. The second step optimizes the uniformity of the pure phase element. The efficiency is only slightly reduced. The theoretical efficiency for a perfectly uniform 9 beam fan-out is better than 99%.

Both optimization steps are very fast compared with other methods. The computing time for a 9 beam element is about 250 ms for the first step and 900 ms for the second step on a MicroVAX 3400. Our optimization parameters are defined in the object plane. Generally, optimization in the hologram plane requires more parameters and consequently more computing power.

The optimization method is easily extendable to large and to two-dimensional fan-outs. Good starting parameters, and therefore short computing time, for large fan-outs are obtained by cascading optimum solutions of smaller fan-outs. The optimum solution for a 117 beam fan-out with 97.6% efficiency and less than 0.1% uniformity error has been obtained from cascading the two optimized solutions for a 9 beam and a 13 beam fan-out.

We have recorded an optimized 9 beam fan-out as a surface relief kinoform with a laser-beam writing system. The implemented phase results from the first optimization step and has a theoretical efficiency of 99.38% and a uniformity of ±5.35%. This element has been investigated experimentally. It shows a high efficiency (92%) and a moderate uniformity (±7%), which is mainly due to fabrication tolerances.

VIII. References

1. J. N. Mait, "Design of binary-phase and multiphase Fourier gratings for array generation," J. Opt. Soc. Am. A 7, 1514–1528 (1990).
2. J. Turunen, J. Fagerholm, A. Vasara, M. R. Taghizadeh, "Detour-phase kinoform interconnects: the concept and fabrication considerations," J. Opt. Soc. Am. A 7, 1202–1208 (1990).
3. M. T. Gale, G. K. Lang, J. M. Raynor, H. Schütz, "Fabrication of microoptical components by laser writing in photoresist," *ECO4*, Proc. SPIE, **1506** (1991).
4. M. T. Gale, G. K. Lang, J. M. Raynor, H. Schütz,"Fabrication of kinoform structures for optical computing," (same issue).
5. H. P. Herzig, R. Dändliker, J. M. Teijido, "Beam shaping for high power laser diode arrays by holographic optical elements", *Holographic Systems, Components and Applications, Bath UK*, Conference Publication Number 311 (IEE, London), 133–137 (1989).
6. H. P. Herzig, D. Prongué, R. Dändliker, "Design and fabrication of highly efficient fan-out element," Jpn. J. Appl. Phys. 27, L1307–L1309 (1990).
7. W. H. Press, B. P. Flannery, S. A. Teukolsky, W. T. Vetterling, "Numerical recipes in pascal," Cambridge University Press (1989)
8. F. Wyrowski, "Diffractive optical elements: iterative calculation of quantized, blazed phase structures," J. Opt. Soc. Am. A 7, 961–969 (1990).

Liste des publications

- H. P. Herzig, D. Prongué, R. Dändliker, "Design and fabrication of highly efficient fan-out element," Jpn. J. Appl. Phys. **27**, L1307-L1309 (1990).
- H. P. Herzig, P. Ehbets, D. Prongué, R. Dändliker, "Fan-out elements by multiple beam recording in volume holograms," *Holographic Optics III: Principles and Applications*, G. M. Morris, ed., Proc. SPIE **1507**, 247-255 (1991).
- H. P. Herzig, P. Ehbets, D. Prongué, R. Dändliker, "Fan-out elements recorded as volume holograms: optimized recording conditions," Appl. Opt. **31**, xxxx-xxxx (1992).
- D. Prongué, H. P. Herzig, "HOE for clock distribution in integrated circuits: Experimental results," *Optical Interconnections and Networks*, Proc. SPIE **1281**, 113-122 (1990).
- D. Prongué, H. P. Herzig, R. Dändliker, M. T. Gale, "Optimized kinoform structures for highly efficient fan-out elements," Appl. Opt. **31**, xxxx-xxxx (1992).

Le texte complet de la thèse est déposé à la bibliothèque de l'Institut de Microtechnique de l'Université de Neuchâtel.